Relativistic nuclear energy density functional constrained by low-energy QCD ⋆

P. Finelli [a], N. Kaiser [a], D. Vretenar [b], W. Weise [a]

[a] *Physik-Department, Technische Universität München, D-85747 Garching, Germany*

[b] *Physics Department, Faculty of Science, University of Zagreb, 10 000 Zagreb, Croatia*

Abstract

A relativistic nuclear energy density functional is developed, guided by two important features that establish connections with chiral dynamics and the symmetry breaking pattern of low-energy QCD: a) strong scalar and vector fields related to in-medium changes of QCD vacuum condensates; b) the long- and intermediate-range interactions generated by one-and two-pion exchange, derived from in-medium chiral perturbation theory, with explicit inclusion of $\Delta(1232)$ excitations. Applications are presented for binding energies, radii of proton and neutron distributions and other observables over a wide range of spherical and deformed nuclei from ^{16}O to ^{210}Po. Isotopic chains of Sn and Pb nuclei are studied as test cases for the isospin dependence of the underlying interactions. The results are at the same level of quantitative comparison with data as the best phenomenological relativistic mean-field models.

Key words: Relativistic Mean Field, Density Functional Theory, Nuclear Structure, Chiral Dynamics, QCD Sum Rules
PACS: 21.10.Dr, 21.30.Fe, 21.60.Jz

1 Introduction.

The successes of modern nuclear structure models in predicting many new phenomena in regions of exotic nuclei far from stability, and the recent applications of chiral effective field theory to nucleon-nucleon scattering and the

⋆ Work supported in part by BMBF, DFG, GSI and MURST.

few-body problem, have highlighted one of the fundamental problems in theoretical nuclear physics: the relationship between low-energy, non-perturbative QCD and the rich structure of nuclear many-body systems.

The most complete and accurate description of structure phenomena in heavy nuclei is currently provided by self-consistent non-relativistic and relativistic mean-field approaches. By employing phenomenological effective interactions, adjusted to empirical properties of symmetric and asymmetric nuclear matter, and to bulk properties of stable nuclei, self-consistent mean-field methods have achieved a high level of precision in describing ground states and properties of excited states in stable nuclei, exotic nuclei far from β-stability, and in nuclear systems at the nucleon drip-lines [1,2].

The self-consistent mean-field approach to nuclear structure represents an approximate implementation of Kohn-Sham density functional theory (DFT) [3,4,5,6]. The DFT provides a description of the nuclear many-body problem in terms of an energy density functional, $E[\rho]$. Mean-field models approximate the exact energy functional which includes all higher-order correlations. A major goal of nuclear structure theory is to build an energy density functional which is universal [3], in the sense that the same functional is used for all nuclei, with the same set of parameters. This framework should then provide a reliable microscopic description of infinite nuclear and neutron matter, ground-state properties of bound nuclei, rotational spectra, low-energy vibrations and large-amplitude adiabatic properties [7].

In order to formulate a microscopic nuclear energy density functional, one must be able to go beyond the mean-field approximation and systematically calculate the exchange-correlation part, $E_{\rm xc}[\rho]$, of the energy functional, starting from the relevant active degrees of freedom at low energy. The *exact* $E_{\rm xc}$ includes all many-body effects. Thus the usefulness of DFT crucially depends on our ability to construct accurate approximations to the exact exchange-correlation energy. The natural microscopic framework is chiral effective field theory. It is based on the separation of scales between long-range pion-nucleon dynamics, described explicitly, and short-distance interactions not resolved in detail at low energies.

An extensive program, synthesizing effective field theory methods and density functional theory, has recently been initiated by Furnstahl and collaborators [8,9,10]. For a dilute, confined Fermi system with short-range interactions, an effective action formalism leads to a Kohn-Sham density functional by applying an inversion method order-by-order in the relevant small expansion parameter, the local Fermi momentum times the scattering length. The starting point is a generating functional with external sources coupled to composite Fermion operators, e.g. particle number densities and kinetic energy densities. A functional Legendre transformation with respect to source fields leads

to an effective action functional from which the energy density functional is calculated.

An alternative approach to the nuclear energy density functional, emphasizing links with low-energy QCD and its symmetry breaking pattern, has recently been introduced [11,12]. It is based on the following conjectures:

(1) The nuclear ground state is characterized by strong scalar and vector mean fields which have their origin in the in-medium changes of the scalar quark condensate (the chiral condensate) and of the quark density.
(2) Nuclear binding and saturation arise primarily from chiral (pionic) fluctuations (reminiscent of van der Waals forces) in combination with Pauli blocking effects and three-nucleon (3N) interactions, superimposed on the condensate background fields and calculated according to the rules of in-medium chiral perturbation theory (ChPT).

The starting point is the description of nuclear matter based on the chiral effective Lagrangian with pions and nucleons [13,14,15,16], recently improved by including explicit $\Delta(1232)$ degrees of freedom [17]. The relevant "small" scales are the Fermi momentum k_f, the pion mass m_π and the $\Delta - N$ mass difference $\Delta \equiv M_\Delta - M_N \simeq 2.1 m_\pi$, all of which are well separated from the characteristic scale of spontaneous chiral symmetry breaking, $4\pi f_\pi \simeq 1.16$ GeV with the pion decay constant $f_\pi = 92.4$ MeV. The calculations have been performed to three-loop order in the energy density. They incorporate the one-pion exchange Fock term, iterated one-pion exchange and irreducible two-pion exchange, including one or two intermediate Δ's. The resulting nuclear matter equation of state is given as an expansion in powers of the Fermi momentum k_f. The expansion coefficients are functions of k_f/m_π and Δ/m_π, the dimensionless ratios of the relevant small scales. Divergent momentum space loop integrals are regularized by introducing subtraction constants in the spectral representations of these terms [17]. The (few) subtraction constants are the only parameters in this approach. They equivalently correspond to two- and three-nucleon contact interactions (and derivatives thereof), encoding short-distance dynamics not resolved in detail at the characteristic momentum scale $k_f \ll 4\pi f_\pi$. The finite parts of the energy density, written in closed form as functions of k_f/m_π and Δ/m_π, represent long and intermediate range (chiral) dynamics with input fixed entirely in the πN sector. The low-energy constants (contact terms) are adjusted to reproduce basic properties of symmetric and asymmetric nuclear matter.

A first version (not yet including explicitly the $\Delta(1232)$) of this microscopic approach has been tested in the analysis of bulk and single-nucleon properties of finite nuclei [11,12]. It was shown that chiral (two-pion exchange) fluctuations play a prominent role in nuclear binding and in the saturation mechanism, while additional strong scalar and vector mean fields of about equal

magnitude and opposite sign, induced by changes of the QCD vacuum in the presence of baryonic matter, generate the large effective spin-orbit potential in finite nuclei. A first series of promising results for $N \approx Z$ nuclei demonstrated that such an approach to nuclear dynamics, constrained by the chiral symmetry breaking pattern and the condensate structure of low-energy QCD, has the capability of describing finite nuclei and their properties at a quantitative level comparable with phenomenological self-consistent mean-field models.

Chiral effective field theories are systematically improved by introducing explicit $\Delta(1232)$ degrees of freedom. Much better isospin properties of nuclear matter are found by including chiral $\pi N\Delta$-couplings [17]. This has an ameliorating influence on the isovector channel of the nuclear energy density functional for finite nuclei, and much improved results are expected for ground-state properties of $N \neq Z$ nuclei. In the present work the effects of the inclusion of chiral $\pi N\Delta$-dynamics on the nuclear energy density functional will be investigated. Specifically, the chiral nuclear matter energy density functional will be mapped onto the exchange-correlation energy density functional of a covariant point-coupling model for finite nuclei, including gradient corrections. This model will be employed in the description of ground-state properties of a broad range of spherical and deformed nuclei. The results will be analyzed in comparison with experimental data on binding energies, charge radii, neutron radii and deformation parameters for several isotopic chains.

In Section 2 we construct the nuclear energy density functional based on the conjectures mentioned previously. Next, in order to deal with a broad range of finite (medium-heavy and heavy) nuclei, it is convenient to formulate an equivalent covariant point-coupling model with density-dependent contact interactions. The mapping of the nucleon self-energies in nuclear matter, calculated using chiral dynamics, onto those of the point coupling model for finite nuclei and the fine-tuning of the remaining parameters is described in Section 3. In Section 4 the resulting self-consistent equations are solved for ground-state properties of a number of spherical and deformed nuclei. Section 5 summarizes the results of the present investigations and ends with an outlook for future studies.

2 The nuclear energy density functional

2.1 Framework and conjectures

It is useful first to recall some basics of (non-relativistic) Density Functional Theory (DFT) [3,4,5,6] for fermionic many-body systems. The starting point of DFT is the Hohenberg-Kohn (HK) variational principle for the ground-state

energy of interacting fermions:

$$E = \min_{\rho}\{F_{\rm HK}[\rho]\} \ . \tag{1}$$

The exact ground-state energy is obtained from the universal functional F_{HK} depending only on the local density $\rho(\mathbf{r})$. The Kohn-Sham DFT considers an auxiliary system of non-interacting quasi-particles and states that for any interacting system, there exists a local single-particle potential (the Kohn-Sham potential) such that the exact ground-state density of the interacting system equals the ground-state density of the auxiliary problem. The HK free energy is commonly decomposed into three separate terms:

$$F_{\rm HK}[\rho] = E_{\rm kin}[\rho] + E_{\rm H}[\rho] + E_{\rm xc}[\rho] \ , \tag{2}$$

where $E_{\rm kin}$ is the kinetic energy of the non-interacting N-particle system, $E_{\rm H}$ is a Hartree energy, and $E_{\rm xc}$ denotes the exchange-correlation energy which, by definition, contains everything else. The practical usefulness of the Kohn-Sham scheme depends entirely on whether accurate approximations for $E_{\rm xc}$ can be found. The local ground-state density is constructed using so-called auxiliary orbitals,

$$\rho(\mathbf{r}) = \sum_{k=1}^{N} |\psi_{KS}^{k}(\mathbf{r})|^2 \ , \tag{3}$$

which are unique functionals of the density $\rho(\mathbf{r})$, i.e. the KS scheme defines a self-consistency problem. The set $\{\psi_{KS}^{k}\}$ of single-particle wave functions represents an "effective" basis because, in general, these functions do not have a directly observable physical interpretation [1] . The corresponding Kohn-Sham single-particle equations, which determine ψ_{KS}^{k}, are easy to solve numerically, even for large numbers of particles. The relativistic analogue of the Kohn-Sham scheme, used in the present work, starts with a set of Dirac spinors $\{\psi_{D}^{k}\}$ which replaces the non-relativistic wave functions $\{\psi_{KS}^{k}\}$.

The conjectures on which our approach to the nuclear energy density functional is based, with contact to low-energy QCD (see Sec. 1), can now be adapted as follows:

(1) The large scalar and vector mean fields (with opposite signs) that have their origin in the in-medium changes of the chiral condensate and of the quark density, determine the Hartree energy functional $E_{\rm H}[\rho]$.

[1] except for the last occupied orbital (see Ref. [6]).

(2) The chiral (pionic) fluctuations including one- and two-pion exchange with single and double virtual $\Delta(1232)$-isobar excitations plus Pauli blocking effects, determine the exchange-correlation energy functional $E_{\rm xc}[\rho]$.

Note that we do not introduce explicit spin orbit terms. They emerge naturally from the Lorentz scalar and vector self-energies generated by the relativistic density functional, as discussed in the following section. Furthermore, contact terms from regularization-dependent pieces of two-pion exchange processes can be grouped together with the Hartree part $E_{\rm H}$ and need not be included in $E_{\rm xc}$. However, we prefer to keep them along with the pionic fluctuations for convenience.

2.2 Density-dependent point coupling approach

The density distribution and the energy of the nuclear ground state are obtained from self-consistent solutions of the relativistic generalizations of the linear single-nucleon Kohn-Sham equations. In order to derive those equations it is useful to construct a point-coupling model [18,19,20] with density dependent interaction terms, designed such as to reproduce the detailed density dependence of the nucleon self-energies resulting from $E_{\rm H}[\rho] + E_{\rm xc}[\rho]$.

The spin-orbit force in nuclei is well known to be abnormally strong. An estimate based on the relation familiar from atoms,

$$\Delta H_{ls} = \frac{\mathbf{l}\cdot\mathbf{s}}{2M_N^2 r}\frac{dU}{dr} \tag{4}$$

using the average nuclear single particle potential U, would give a spin-orbit interaction too weak by about an order of magnitude. It is also known [17] that chiral one- and two-pion exchange dynamics alone cannot reproduce the observed $\mathbf{l}\cdot\mathbf{s}$ interaction. Additional mechanisms are required, such as the coherent action of strong scalar and vector potentials in relativistic mean-field models. In order to generate the large empirical spin-orbit splittings, we have two options. The first one is to stay within a non-relativistic framework (such as the Skyrme energy density functional) and simply fix the spin-orbit coupling by an appropriate contact term. The second option (the one we adopt here) is to preserve the distinction between scalar and vector nucleon self-energies in a relativistic description.

In the effective field theory approach to the NN interaction [21] short range central and spin-orbit forces are represented by contact interactions with low-energy parameters fitted to NN phase shifts. It has been demonstrated in [22] how these low-energy parameters translate into an equivalent Skyrme repre-

sentation and - not surprisingly - account for the correct magnitude of the spin-orbit force as required already for the fit to triplet p-wave NN phase shifts. In our approach the role of these contact terms is taken over by the strong Lorentz scalar and vector fields which produce effectively the same spin-orbit coupling at the level of the nuclear mean field.

A successful framework that meets these requirements for a two component system of protons and neutrons starts from a relativistic Lagrangian which includes isoscalar-scalar (S), isoscalar-vector (V), isovector-scalar (TS) and isovector-vector (TV) effective four-fermion interaction vertices with density-dependent coupling strengths. The density dependence represents many-body effects beyond mean field and two-body forces, including Pauli blocking effects. In Refs. [11,12] we have shown that a very good description of nuclear matter and finite nuclei from oxygen to calcium can be based on the following minimal Lagrangian density:

$$\mathcal{L} = \mathcal{L}_{\rm free} + \mathcal{L}^{(1)}_{\rm int} + \mathcal{L}^{(2)}_{\rm int} + \mathcal{L}_{\rm coul}, \tag{5}$$

The four terms read:

$$\mathcal{L}_{\rm free} = \bar\psi(i\gamma_\mu\partial^\mu - M_N)\psi \ , \tag{6}$$

$$\begin{aligned}\mathcal{L}^{(1)}_{\rm int} = &-\frac{1}{2}\ G_S(\hat\rho)(\bar\psi\psi)(\bar\psi\psi) - \frac{1}{2}\ G_V(\hat\rho)(\bar\psi\gamma_\mu\psi)(\bar\psi\gamma^\mu\psi) \\ &-\frac{1}{2}\ G_{TS}(\hat\rho)(\bar\psi\vec\tau\psi)\cdot(\bar\psi\vec\tau\psi) - \frac{1}{2}\ G_{TV}(\hat\rho)(\bar\psi\vec\tau\gamma_\mu\psi)\cdot(\bar\psi\vec\tau\gamma^\mu\psi)\ ,\end{aligned} \tag{7}$$

$$\mathcal{L}^{(2)}_{\rm int} = -\frac{1}{2}\ D_S\partial_\nu(\bar\psi\psi)\partial^\nu(\bar\psi\psi)\ , \tag{8}$$

$$\mathcal{L}_{\rm em} = eA^\mu\bar\psi\frac{1+\tau_3}{2}\gamma_\mu\psi - \frac{1}{4}F_{\mu\nu}F^{\mu\nu}\ , \tag{9}$$

where ψ is the Dirac field of the nucleon with its two isospin components (p and n). Vectors in isospin space are denoted by arrows. In addition to the free nucleon Lagrangian $\mathcal{L}_{\rm free}$ and the interaction terms contained in $\mathcal{L}^{(1)}_{\rm int}$, when applied to finite nuclei, the model must include the coupling $\mathcal{L}_{\rm em}$ of the protons to the electromagnetic field A^μ with $F_{\mu\nu} = \partial_\mu A_\nu - \partial_\nu A_\mu$, and a derivative (surface) term $\mathcal{L}^{(2)}_{\rm int}$. One could, of course, construct additional derivative terms in $\mathcal{L}^{(2)}_{\rm int}$, further generalized to include density dependent strength parameters. However, as we shall see, there appears to be no need in practical applications to go beyond the simplest ansatz (8) with a constant D_S. In fact, present data on nuclear ground states constrain only this single isoscalar derivative term [23].

The variational principle $\delta\mathcal{L}/\delta\bar\psi = 0$ applied to the Lagrangian (5) leads to the self-consistent single-nucleon Dirac equations, the relativistic analogue of

the (non-relativistic) Kohn-Sham equations. The nuclear dynamics produced by chiral (pionic) fluctuations in the medium is now encoded in the density dependence of the interaction vertices.

In the framework of relativistic density functional theory [6,24,25,26], the density-dependent couplings are functions of the 4-current j^μ:

$$j^\mu = \bar{\psi}\gamma^\mu\psi = \hat{\rho}u^\mu \ , \tag{10}$$

where u^μ is the 4-velocity defined as $(1-\boldsymbol{v}^2)^{-1/2}(1,\boldsymbol{v})$. We work in the rest-frame of the nuclear system with $\boldsymbol{v}=0$.

The couplings $G_i(\hat{\rho})$ $(i = S, V, TS, TV)$ are decomposed as follows:

$$\begin{aligned} & G_i(\hat{\rho}) = G_i^{(0)} + G_i^{(\pi)}(\hat{\rho}) \quad (\text{for } i = S, V) \\ \text{and} \quad & G_i(\hat{\rho}) = G_i^{(\pi)}(\hat{\rho}) \qquad\quad (\text{for } i = TS, TV) \ , \end{aligned} \tag{11}$$

into density-independent parts $G_i^{(0)}$ which arise from strong isoscalar scalar and vector background fields, and density-dependent parts $G_i^{(\pi)}(\hat{\rho})$ generated by (regularized) one- and two-pion exchange dynamics. As in our previous work, it is assumed that only pionic processes contribute to the isovector channels.

The relativistic density functional describing the ground-state energy of the system can be re-written as a sum of four distinct terms:

$$E_0[\hat{\rho}] = E_{\rm free}[\hat{\rho}] + E_{\rm H}[\hat{\rho}] + E_{\rm coul}[\hat{\rho}] + E_\pi[\hat{\rho}] \ , \tag{12}$$

with

$$E_{\rm free}[\hat{\rho}] = \int d^3r \ \langle\phi_0|\bar{\psi}[-i\boldsymbol{\gamma}\cdot\boldsymbol{\nabla} + M_N]\psi|\phi_0\rangle \ , \tag{13}$$

$$E_{\rm H}[\hat{\rho}] = \frac{1}{2}\int d^3r \ \{\langle\phi_0|G_S^{(0)}(\bar{\psi}\psi)^2|\phi_0\rangle + \langle\phi_0|G_V^{(0)}(\bar{\psi}\gamma_\mu\psi)^2|\phi_0\rangle\} \ , \tag{14}$$

$$\begin{aligned} E_\pi[\hat{\rho}] = \frac{1}{2}\int d^3r \ \Big\{ & \langle\phi_0|G_S^{(\pi)}(\hat{\rho})(\bar{\psi}\psi)^2|\phi_0\rangle + \langle\phi_0|G_V^{(\pi)}(\hat{\rho})(\bar{\psi}\gamma_\mu\psi)^2|\phi_0\rangle \\ & + \langle\phi_0|G_{TS}^{(\pi)}(\hat{\rho})(\bar{\psi}\vec{\tau}\psi)^2|\phi_0\rangle + \langle\phi_0|G_{TV}^{(\pi)}(\hat{\rho})(\bar{\psi}\gamma_\mu\vec{\tau}\psi)^2|\phi_0\rangle \\ & - \langle\phi_0|D_S^{(\pi)}[\boldsymbol{\nabla}(\bar{\psi}\psi)]^2|\phi_0\rangle\Big\} \ , \end{aligned} \tag{15}$$

$$E_{coul}[\hat{\rho}] = \frac{1}{2}\int d^3r \ \langle\phi_0|A^\mu e\bar{\psi}\frac{1+\tau_3}{2}\gamma_\mu\psi|\phi_0\rangle \quad , \tag{16}$$

where $|\phi_0\rangle$ denotes the nuclear ground state. Here $E_{\rm free}$ is the energy of the free (relativistic) nucleons including their rest mass. $E_{\rm H}$ is a Hartree-type

contribution representing strong scalar and vector mean fields, later to be connected with the leading terms of the corresponding nucleon self-energies deduced from in-medium QCD sum rules. Furthermore, E_π is the part of the energy generated by chiral $\pi N\Delta$-dynamics, including a derivative (surface) term, with all pieces explicitly derived in [17].

Note that Eqs. (12-16) are arranged in close correspondence with a relativistic extension of the Hohenberg-Kohn energy functional (2), identifying the Hartree term $E_{\rm H}$ with Eq. (14) plus the Coulomb energy (16), and the exchange correlation part with E_π of Eq. (15). Minimization of the ground-state energy, represented in terms of a set of auxiliary Dirac spinors ψ_k, leads to the relativistic analogue of the Kohn-Sham equations. These single-nucleon Dirac equations are solved self-consistently in the "no-sea" approximation which omits the explicit contribution of the negative-energy solutions of the relativistic equations to the densities and currents. This means that vacuum polarization effects are not taken into account explicitly. They are included in the adjustable parameters of the theory (for an exhaustive discussion see Refs. [24,27,28,29]). This no-sea approximation is well founded within the framework of an effective field theory. Nucleon-antinucleon fluctuations occur at high-energy (short-distance) scales, not resolved at the long wavelength characteristic of the nuclear Fermi momentum. Such fluctuations are implicitly absorbed, together with other short-range dynamics, in contact terms of the effective Lagrangian.

The expressions for the isoscalar and isovector four-currents and scalar densities read:

$$j_\mu = \langle\phi_0|\bar\psi\gamma_\mu\psi|\phi_0\rangle = \sum_{k=1}^{N}\bar\psi_k\gamma_\mu\psi_k \ , \tag{17}$$

$$\vec{j}_\mu = \langle\phi_0|\bar\psi\gamma_\mu\vec\tau\psi|\phi_0\rangle = \sum_{k=1}^{N}\bar\psi_k\gamma_\mu\vec\tau\psi_k \ , \tag{18}$$

$$\rho_S = \langle\phi_0|\bar\psi\psi|\phi_0\rangle = \sum_{k=1}^{N}\bar\psi_k\psi_k \ , \tag{19}$$

$$\vec\rho_S = \langle\phi_0|\bar\psi\vec\tau\psi|\phi_0\rangle = \sum_{k=1}^{N}\bar\psi_k\vec\tau\psi_k \ , \tag{20}$$

where ψ_k are Dirac spinors and the sum runs over occupied positive-energy single-nucleon states.

In this work we only consider systems with time-reversal symmetry in the ground-state, i.e. even-even nuclei. The space components of all currents vanish ($\mathbf{j} = 0$), and because of charge conservation only the third component of isospin ($\tau_3 = -1$ for neutrons and $\tau_3 = +1$ for protons) contributes. The relevant

combinations of densities are:

$$\rho = \langle\phi_0|\bar{\psi}\gamma^0\psi|\phi_0\rangle = \rho^p + \rho^n \ , \tag{21}$$
$$\rho_3 = \langle\phi_0|\bar{\psi}\tau_3\gamma^0\psi|\phi_0\rangle = \rho^p - \rho^n \ , \tag{22}$$
$$\rho_S = \langle\phi_0|\bar{\psi}\psi|\phi_0\rangle = \rho_S^p + \rho_S^n \ , \tag{23}$$
$$\rho_{S3} = \langle\phi_0|\bar{\psi}\tau_3\psi|\phi_0\rangle = \rho_S^p - \rho_S^n \ . \tag{24}$$

The charge density is

$$\rho_{ch} = \langle\phi_0|\bar{\psi}\gamma^0\frac{1+\tau_3}{2}\psi|\phi_0\rangle = \rho^p \ .$$

The single-nucleon Dirac equation is found by minimization with respect to $\bar{\psi}_k$:

$$[-i\boldsymbol{\gamma}\cdot\boldsymbol{\nabla} + M_N + \gamma_0\Sigma_V + \gamma_0\tau_3\Sigma_{TV} + \gamma_0\Sigma_R + \Sigma_S + \tau_3\Sigma_{TS}]\psi_k = \epsilon_k\psi_k \ , \tag{25}$$

with the self-energies:

$$\Sigma_V = [G_V^{(0)} + G_V^{(\pi)}(\rho)]\rho + eA^0\frac{1+\tau_3}{2} \ , \tag{26}$$
$$\Sigma_{TV} = G_{TV}^{(\pi)}(\rho)\,\rho_3 \ , \tag{27}$$
$$\Sigma_S = [G_S^{(0)} + G_S^{(\pi)}(\rho)]\rho_S + D_S^{(\pi)}\boldsymbol{\nabla}^2\rho_S \ , \tag{28}$$
$$\Sigma_{TS} = G_{TS}^{(\pi)}(\rho)\,\rho_{S3} \ , \tag{29}$$
$$\Sigma_R = \frac{1}{2}\left\{\frac{\partial G_V^{(\pi)}(\rho)}{\partial\rho}\rho^2 + \frac{\partial G_S^{(\pi)}(\rho)}{\partial\rho}\rho_S^2 + \frac{\partial G_{TV}^{(\pi)}(\rho)}{\partial\rho}\rho_3^2 + \frac{\partial G_{TS}^{(\pi)}(\rho)}{\partial\rho}\rho_{S3}^2\right\} \ , \tag{30}$$

where $A^0(\mathbf{r}) = \frac{e}{4\pi}\int d^3r' \ \frac{\rho_{ch}(\mathbf{r}')}{|\mathbf{r}-\mathbf{r}'|}$ is the Coulomb potential. In addition to the usual contributions from the time components of the vector self-energies and the scalar potentials, we must also include the "rearrangement" terms, Σ_R, arising from the variation of the vertex functionals with respect to the nucleon fields in the density operator $\hat{\rho}$. For a Lagrangian with density dependent couplings, the inclusion of the rearrangement self-energies is essential in order to guarantee energy-momentum conservation and thermodynamical consistency [30,31,32]. It is also required by the Hugenholtz-Van Hove theorem [33]. Using the single-nucleon Dirac equation and performing an integration by parts, the ground-state energy of a nucleus with A nucleons reads:

$$E_0 = \sum_{k=1}^{A} \epsilon_k \;\; -\frac{1}{2}\int d^3r \Big\{ \; [G_S^{(0)} + G_S^{(\pi)}(\rho)]\, \rho_S^2 + G_{TS}^{(\pi)}(\rho)\, \rho_{S3}^2 + [G_V^{(0)} + G_V^{(\pi)}(\rho)]\, \rho^2 + G_{TV}^{(\pi)}(\rho)\, \rho_3^2 + \frac{\partial G_S^{(\pi)}(\rho)}{\partial \rho}\, \rho_S^2\, \rho + \frac{\partial G_{TS}^{(\pi)}(\rho)}{\partial \rho}\, \rho_{S3}^2\, \rho + \frac{\partial G_V^{(\pi)}(\rho)}{\partial \rho}\, \rho^3 + \frac{\partial G_{TV}^{(\pi)}(\rho)}{\partial \rho}\, \rho_3^2\, \rho + e\, \rho_{ch}\, A^0 + D_S^{(\pi)} \rho_S \nabla^2 \rho_S \Big\} \;, \tag{31}$$

where ϵ_k denotes the single-nucleon energies.

3 Linking the energy functional to the low-energy sector of QCD.

3.1 Scalar and vector fields: guidance from in-medium QCD sum rules.

The QCD ground state (or "vacuum") is characterized by strong condensates of quark-antiquark pairs and gluons, an entirely non-perturbative phenomenon. The quark condensate $\langle \bar{q} q \rangle$, i.e. the ground state expectation value of the scalar quark density, plays a particularly important role as an order parameter of spontaneously broken chiral symmetry. At a renormalization scale of about 1 GeV (with up and down quark masses $m_u + m_d \simeq 12$ MeV) the value of the chiral vacuum condensate [34] is $\langle \bar{q} q \rangle_0 \simeq -(240 \text{ MeV})^3 \simeq -1.8 \text{ fm}^{-3}$. Hadrons, as well as nuclei, are excitations built on this condensed ground state. Changes of the condensate structure of the QCD vacuum in the presence of baryonic matter are a source of strong fields experienced by the nucleons in the bulk of nuclei.

In-medium QCD sum rules relate the leading changes of the scalar quark condensate and of the quark density at finite baryon density, with the scalar and vector self-energies of a nucleon in the nuclear medium. To first order in the scalar and baryon densities, these self-energies can be expressed as follows [12,35,36,37,38,39]:

$$\Sigma_S^{(0)} = -\frac{\sigma_N M_N}{m_\pi^2 f_\pi^2} \rho_S \;, \tag{32}$$

$$\Sigma_V^{(0)} = \frac{4(m_u + m_d) M_N}{m_\pi^2 f_\pi^2} \rho \;, \tag{33}$$

where $\sigma_N = \langle N | m_q\, \bar{q} q | N \rangle$ is the nucleon sigma term ($\simeq 50$ MeV), m_π is the pion mass (138 MeV), and $f_\pi = 92.4$ MeV is the pion decay constant. The

resulting $\Sigma_S^{(0)}$ and $\Sigma_V^{(0)}$ are individually of the order of 300 – 400 MeV in magnitude. Their ratio

$$\frac{\Sigma_S^{(0)}}{\Sigma_V^{(0)}} = -\frac{\sigma_N}{4(m_u+m_d)}\frac{\rho_S}{\rho} \tag{34}$$

is close to -1, suggesting a large cancellation of scalar and vector potentials in the single-nucleon Dirac equation, a feature characteristic of relativistic mean-field phenomenology. Of course the constraints implied by Eqs. (32)-(33), and by the ratio Eq. (34) are not very accurate on a quantitative level. Beyond the leading-order Ioffe formula [40] on which Eq. (32) is based, one finds corrections from condensates of higher dimension which are not well under control. Given in addition the uncertainties in the values of σ_N and $m_u + m_d$, the estimated error for the ratio $\Sigma_S^{(0)}/\Sigma_V^{(0)} \simeq -1$ is about 20%. It is important to note, however, that the explicitly calculated two-pion exchange fluctuations, used in this work, account for a large part of the effects from higher dimensional condensates (such as the four-quark condensate). Restricting $\Sigma_{S,V}^{(0)}$ to the leading order terms (32-33) does therefore make sense.

Comparing Eqs. (26) and (28) for the isoscalar vector and scalar potentials of the single-nucleon Dirac equations, with the Eqs. (32) and (33) for the condensate background self-energies, respectively, the following estimates hold for the couplings of the nucleon to the background fields (the Hartree terms in the energy functional):

$$G_S^{(0)} = -\frac{\sigma_N M_N}{m_\pi^2 f_\pi^2}\ , \tag{35}$$

and

$$G_V^{(0)} = \frac{4(m_u+m_d)M_N}{m_\pi^2 f_\pi^2}\ . \tag{36}$$

Inserting the values of the nucleon and pion masses and the pion decay constant,

$$G_S^{(0)} \simeq -11\ \text{fm}^2\ \left[\frac{\sigma_N}{50\ \text{MeV}}\right]\ , \tag{37}$$

$$G_V^{(0)} \simeq 11\ \text{fm}^2\ \left[\frac{4(m_u+m_d)}{50\ \text{MeV}}\right]\ , \tag{38}$$

which implies $G_S^{(0)} \simeq -G_V^{(0)} \simeq -10.6\ \text{fm}^2$ for typical values $\sigma_N \simeq 48$ MeV and $m_u+m_d \simeq 12$ MeV (at a renormalization scale of about 1 GeV). This estimate

is useful for first orientation. In the actual applications to finite nuclei, $G_{S,V}^{(0)}$ will have to be fine-tuned. We mention here in advance that, as a remarkable and non-trivial result of this fine-tuning, deviations from the "canonical" values (37-38) will turn out to be surprisingly small.

3.2 The exchange-correlation term: In-medium chiral perturbation theory.

The many-body effects represented by the exchange-correlation density functional are approximated by chiral $\pi N\Delta$-dynamics, including Pauli blocking effects. Our framework is in-medium chiral perturbation theory with inclusion of Δ-isobars, computed to three-loop order in the energy density and described in detail in Refs. [13,14,15,16,17].

Regularization dependent short-range contributions from pion loops are encoded in a few parameters representing counter terms, or equivalently, subtraction constants in spectral representations of the respective momentum space amplitudes. At the level of the effective Lagrangian, they appear as contact interactions or derivatives thereof. The counter-term contributions to the energy per particle, $\bar{E} = E/A - M_N$, in symmetric nuclear matter are written:

$$\Delta\bar{E}(k_f)^{(ct)} = b_3\frac{k_f^3}{\Lambda^2} + b_5\frac{k_f^5}{\Lambda^4} + b_6\frac{k_f^6}{\Lambda^5}\ . \tag{39}$$

At this stage the calculation for homogeneous nuclear matter excludes surface terms which are discussed in the next section. The constants b_i are defined dimensionless, along with a convenient scale Λ to be chosen larger than the "small" scales (k_f, m_π and Δ) but smaller than the "chiral gap", $4\pi f_\pi$. Our choice is $\Lambda = 2\pi f_\pi \simeq 0.58$ GeV.

For asymmetric nuclear matter, the energy per particle is written $\bar{E}_{as} = \bar{E} + \delta^2 S_2$ with the asymmetry energy S_2 and $\delta = (\rho^n - \rho^p)/\rho$. The counter-term contributions to the asymmetry energy has an expansion analogous to (39),

$$\Delta S_2(k_f)^{(ct)} = a_3\frac{k_f^3}{\Lambda^2} + a_5\frac{k_f^5}{\Lambda^4} + a_6\frac{k_f^6}{\Lambda^5}\ , \tag{40}$$

with dimensionless constants a_i. The parameters b_i and a_i subsume unresolved short-distance NN-dynamics in the nuclear medium. Note that no regularization is required at order k_f^4 where the corresponding loop integrals are all finite. There are no contact interactions that generate a k_f^4 term at the Hartree-Fock level; gradient terms start minimally as ∇^2. At order k_f^5 the constants b_5 and a_5 represent short-distance effects partly arising from momentum dependent interactions. In actual practice it turns out that these constants can be set

to zero [17], the primary momentum dependent forces being already well described by the finite parts of in-medium two-pion exchange pieces. Additional short-range three-body contributions and effects of higher loops which feed back into k_f^6 terms are parameterized by the constants b_6 and a_6, respectively.

In Ref. [17] the counter terms b_i and a_i have been adjusted to reproduce nuclear and neutron matter properties. The resulting equation of state of isospin-symmetric matter is in good agreement with recent microscopic calculations [41], though with a somewhat too high incompressibility ($K_0 = 304$ MeV). The calculated real part of the nucleon single-particle potential, $U(p, k_f)$, is very close to the result of relativistic Dirac-Brueckner calculations (see Ref. [42]). Isospin properties of nuclear matter and the energy per particle in neutron matter are significantly improved by incorporating explicit $\pi N\Delta$-dynamics, in comparison with earlier calculations (see Ref. [13]) which included only nucleons in two-pion exchange processes.

While gross properties of infinite nuclear matter are useful for orientation, the large amount of nuclear observables studied in the present work provides a far more accurate data base that permits a better adjustment of the constants b_i and a_i. We refer to the more detailed discussion in Section 3.3 but point here already to the interesting result that the best fit values for b_3 and a_3 turn out to be within only a few percent of those determined in the ChPT calculation of nuclear and neutron matter, while $b_5 = a_5 = 0$ can still be maintained. The only major difference is in the short-distance three-body term proportional to b_6 for which the fit to the broad range of nuclear data requires stronger attraction. Throughout the procedure, the input values for the chiral pion-nucleon and $\pi N\Delta$ couplings are strictly kept fixed by pion-nucleon scattering observables in vacuum. These couplings determine the finite parts of intermediate-range one- and two- pion exchange contributions to the energy density as predicted by in-medium ChPT.

In the simplest DFT approach, the exchange-correlation energy for a finite system is determined in the local density approximation (LDA) from the exchange-correlation functional of the corresponding infinite homogeneous system, replacing the constant density ρ by the local density $\rho(\mathbf{r})$ of the actual inhomogeneous system. In our case the exchange-correlation terms of the nuclear density functional are determined within LDA by equating the corresponding self-energies in the single-nucleon Dirac equation (25), with those arising from the in-medium chiral perturbation theory calculation of $\pi N\Delta$-dynamics in homogeneous isospin symmetric and asymmetric nuclear matter. Steps beyond the LDA will be taken by adding surface terms involving derivatives of the density.

The density-dependent couplings $G_i^{(\pi)}$ are expressed as polynomials in frac-

tional powers of the baryon density:

$$G_i^{(\pi)}(\rho) = c_{i1} + c_{i2}\rho^{\frac{1}{3}} + c_{i3}\rho^{\frac{2}{3}} + c_{i4}\rho \ldots \ (i = S, V, TS, TV) \ . \tag{41}$$

The detailed derivation of the constants c_{ij} is presented in the Appendix.

The coefficient $D_S^{(\pi)}$ of the derivative term in the equivalent point-coupling model (Eqs. (26) and (28)) can be determined from ChPT calculations for inhomogeneous nuclear matter. The density-matrix expansion method [43] is used to derive the in-medium insertion in the nucleon propagator, as shown in Refs. [14,17]. The isoscalar nuclear energy density emerging from chiral pion-nucleon dynamics has the form:

$$\mathcal{E}(\rho, \boldsymbol{\nabla}\rho) = \rho\, \bar{E}(k_f) + (\boldsymbol{\nabla}\rho)^2\, F_\nabla(k_f) + \ldots \ . \tag{42}$$

The coefficients have been compared with the corresponding phenomenological parameters of various Skyrme type energy density functionals. In particular, the gradient term $(\boldsymbol{\nabla}\rho)^2 F_\nabla(k_f)$ plays an important role in shaping the nuclear surface [44]. While the applicability of the density-matrix expansion is questionable at very low densities, an important result of Refs. [14,17] is that around nuclear matter saturation density, the parameter-free ChPT prediction for $F_\nabla(k_{f0})$ is in very good agreement with the empirical values used in standard parameterizations of the Skyrme density functional [1]. We can approximate F_∇ by a constant in the relevant region of densities. The following relationship between F_∇ and the derivative term of the point-coupling model (see Eqs. (8,15)) is then deduced by a straightforward comparison [45]:

$$-2F_\nabla = D_S^{(\pi)} \ . \tag{43}$$

With the average value of $F_\nabla(k_f)$ in the region 0.1 fm$^{-3} \leq \rho \leq$ 0.2 fm^{-3} [17], we estimate $D_S^{(\pi)} = -0.7$ fm^4.

The inclusion of derivative terms in the model Lagrangian and the determination of its strength parameters from ChPT calculations in inhomogeneous matter actually goes beyond the local density approximation. The term, Eq. (8), with the strength parameter given by Eq. (43), represents a second-order gradient correction to the LDA, i.e. the next-to-leading term in the gradient expansion of the exchange-correlation energy calculated by in-medium chiral perturbation theory.

Table 1
Empirical nuclear matter properties (energy per particle, saturation density, incompressibility, Dirac effective mass, symmetry energy) employed in the adjustment of parameters. For each "empirical" quantity we include the range of values within which the quantity was allowed to vary during the fit.

	E/A (MeV)	ρ_{sat} (fm^{-3})	K_0 (MeV)	M^*/M_N	S_2 (MeV)
Fit	-16. ($\pm$1.)	0.15 ($\pm$0.01)	250. ($\pm$25.)	0.6 ($\pm$0.5)	33. ($\pm$3.)

Table 2
Empirical properties of finite nuclei [57,58] employed in the fitting procedure: binding energies (E_b), charge radii (r_{ch}) and differences between r.m.s. neutron and proton radii ($r_n - r_p$). The relative weights used in fitting these quantities are 0.3%, 0.2% and 10% respectively.

	E_b (MeV)	r_{ch} (fm)	$r_n - r_p$ (fm)
^{16}O	-127.62	2.73	—
^{40}Ca	-342.05	3.49	—
^{48}Ca	-415.99	3.48	—
^{72}Ni	-613.17	—	—
^{90}Zr	-783.89	4.27	—
^{116}Sn	-988.68	4.63	0.12
^{124}Sn	-1049.96	4.67	0.19
^{132}Sn	-1102.92	—	—
^{204}Pb	-1607.52	5.49	—
^{208}Pb	-1636.45	5.51	0.20
^{214}Pb	-1663.30	5.56	—
^{210}Po	-1645.23	—	—

3.3 Adjusting parameters

The parameters of the point-coupling model are fixed simultaneously to properties of nuclear matter (see Table 1), and to binding energies, charge radii and differences between neutron and proton radii of spherical nuclei (see Table 2). The inclusion of neutron-rich nuclei, in particular, provides strict constraints for the parameters in the isovector channel. In both tables the empirical values and data are listed together with the relative errors used in the fitting procedure.

Corrections have been applied for center-of-mass motion and pairing. From the solution of the self-consistent equations we subtract the microscopically calculated center-of-mass correction from the total binding energy, following [46]:

$$\Delta E_{cm} = -\frac{\langle P_{cm}^2 \rangle}{2AM_N} \,, \tag{44}$$

where P_{cm}^2 is the total squared momentum of a nucleus with A nucleons. For the open shell nuclei in Table 2, pairing correlations are treated in the BCS approximation with empirical gaps [47].

We have adjusted a minimal set of parameters starting from the estimates Eqs. (37) and (38) for the couplings of the condensate background fields (Hartree term), and the counter term constants b_3, a_3, b_5, a_5 and b_6, a_6 guided by Ref. [17] for the self-energies arising from chiral $\pi N\Delta$-dynamics (exchange-correlation term). In particular we set $b_5 = a_5 = 0$ as in Ref. [17]. The total number of adjustable parameters is seven. However, five of those will turn out to be remarkably close to preceding expectations or predictions. Only the two constants associated with three-body correlations are free of links to other constraints.

The resulting optimal parameter set (FKVW) is shown in Table 3 in comparison with estimates and predictions: a) for the Hartree term from in-medium QCD sum rules; b) for the exchange-correlation functional from the in-medium ChPT calculations of $\pi N\Delta$-dynamics in nuclear matter.

Evidently the *best fit* parameters are remarkably close to the anticipated QCD sum rule and ChPT values, with the exception of the k_f^6 terms (b_6 and a_6) for which the fit to nuclear data systematically requires an attractive shift as compared to the ChPT calculation [17].

The QCD sum rule predictions for the condensate background scalar and vector self-energies have an accuracy of about 20 % as mentioned previously. Surprisingly, however, the leading-order sum rule estimates, Eqs. (37) and (38), turn out to be realized remarkably well when the parameters of the scalar and vector Hartree fields are varied freely and optimized in confrontation with a large number of high-precision nuclear data. There appears to be an a posteriori consistency with the implicit assumption made in the in-medium ChPT calculations based on $\pi N\Delta$-dynamics: namely that the individually large scalar and vector nucleon self-energies $\Sigma_S^{(0)}$ and $\Sigma_V^{(0)}$ cancel in their contribution to the energy density around saturation. Of course, the b_3 counter term at order k_f^3 from regularized two-pion exchange can be translated into an equivalent Hartree term as well, such that the total balance of scalar and vector self-energy contributions linear in density is attractive and reminiscent

Table 3
Best-fit parameters of the density-dependent point coupling model (Fit FKVW). Upper panel: coupling strengths of background (Hartree) terms in comparison with estimates from in-medium QCD sum rules (37, 38) (QCDSR). Lower panel: constants of counter terms from short-distance regularization (reference scale $\Lambda = 2\pi f_\pi \simeq 0.58$ GeV) and surface (derivative) term $D_S^{(\pi)}$ in comparison with results from in-medium ChPT at three-loop order including $\Delta(1232)$ [17]. The choice $b_5 = a_5 = 0$ from Ref. [17] has been kept, and these parameters are not included in the fitting procedure.

Background (Hartree) terms		
	Fit FKVW	QCDSR
$G_S^{(0)}$ [fm^2]	- 11.5	-10.6
$G_V^{(0)}$ [fm^2]	11.0	10.6
Counter terms / Pionic fluctuations		
	Fit FKVW	ChPT [17]
b_3	-2.93	-3.05
a_3	2.20	2.16
b_5^*	0	0
a_5^*	0	0
b_6	-5.68	-2.83
a_6	-0.13	2.83
$D_S^{(\pi)}$ [fm^4]	-0.76	-0.7
*: inputs, see Ref. [17]		

of QHD and the Walecka model [27]. The repulsive term of order k_f^4 (or $\rho^{4/3}$), on the other hand, results model-independently from Pauli blocking effects on chiral two-pion exchange within in-medium ChPT and has no counterpart in relativistic mean field models.

It is instructive to examine the hierarchy of terms in the k_f-expansion of the nucleon isoscalar single particle potential,

$$U(k_f) = g_3 \frac{k_f^3}{\Lambda^2} + g_4 \frac{k_f^4}{\Lambda^3} + g_5 \frac{k_f^5}{\Lambda^4} + g_6 \frac{k_f^6}{\Lambda^5} + \mathcal{O}(\frac{k_f^7}{\Lambda^6}) \quad , \tag{45}$$

given in detail in the Appendix. The reference scale is chosen again as $\Lambda = 2\pi f_\pi \simeq 0.58$ GeV. The resulting coupling strengths g_i are listed in Table 4. They are all of "natural" size when looked at from the point of view of an effective field theory. Background fields can be ignored here because their

Table 4
Comparison between fine-tuned coefficients g_i (Fit FKVW) in the expansion (45) of the isoscalar single-particle potential, and ChPT values of g_i deduced from calculations performed in Ref. [17]. The constants b_i used in this compilation are those given in Table 3 (see Appendix for further details).

	Fit FKVW	ChPT [17]
g_3	-2.84	-3.10
g_4	2.67	2.67
g_5	2.17	2.17
g_6	-3.35	5.21

contributions to U cancel almost completely, i.e. $U^{(0)} = G_S^{(0)}\rho_S + G_V^{(0)}\rho \simeq 0$.

An alternative way of displaying the convergence properties of the k_f expansion is by translating U of Eq. (45) into the following form of a (local) potential:

$$U(\mathbf{r}) = U_3\frac{\rho(\mathbf{r})}{\rho(0)} + U_4\left(\frac{\rho(\mathbf{r})}{\rho(0)}\right)^{4/3} + U_5\left(\frac{\rho(\mathbf{r})}{\rho(0)}\right)^{5/3} + U_6\left(\frac{\rho(\mathbf{r})}{\rho(0)}\right)^{2} \quad , \qquad (46)$$

where $\rho(0)$ is the central ($\mathbf{r} = 0$) value of the density distribution $\rho(\mathbf{r})$. As a typical example (for $\rho \simeq \rho(0) \simeq \rho_{sat}$) one finds a sequence of coefficients U_n as shown in Fig. 1. Note once again that the leading attractive piece U_3 (proportional to the density ρ) does not receive contributions from the individually much stronger background self-energies $\Sigma_V^{(0)} \simeq -\Sigma_S^{(0)} \simeq 0.35$ GeV which cancel in the energy per particle but coherently build up the large spin-orbit coupling in finite nuclei. The terms of order $\rho^{4/3}$ and $\rho^{5/3}$ (with coefficients U_4 and U_5) are repulsive and successively smaller, while the "three-body" term U_6 proportional to ρ^2 is attractive and even smaller in magnitude.

It might appear that the attractive ρ^2 term causes nuclear matter to collapse at very high density. We have checked that stability persists up to at least three times the density of normal nuclear matter. At even higher densities, expansions such as (45) must be carried to higher orders in k_f. One should recall, however, that the limit of applicability for the present chiral approach is imposed by the condition that k_f must remain sufficiently small compared to the reference scale Λ.

Using the input parameters specified earlier in this section, let us have a look at a first series of results achieved in comparison with data. In Fig. 2 we plot the relative deviations between calculated and experimental values, $((\mathcal{O}^i_{th} - \mathcal{O}^i_{exp})/\mathcal{O}^i_{exp})$ in percent, of binding energies and charge radii for all

nuclei that have been included in the fit (see Tab. 2). The RMF+BCS results obtained with the FKVW parameter set are compared to those of two standard phenomenological relativistic mean-field models using a) the non-linear meson exchange interaction NL3 [48], and b) the density-dependent meson-exchange interaction DD-ME1 [49]. The binding energies and charge radii calculated in the present work are comparable or superior to those produced with two of the most accurate phenomenological relativistic mean-field interactions (the number of free parameters is seven for NL3, and eight for DD-ME1).

4 Ground-state properties of spherical and deformed nuclei

In Ref. [12] a first version of our relativistic point-coupling model (at that stage without explicit inclusion of $\Delta(1232)$ degrees of freedom) has been tested in an analysis of the equations of state for symmetric and asymmetric nuclear matter, and of bulk and single-nucleon properties of light and medium heavy $N \approx Z$ nuclei. The detailed isospin dependence of the effective interaction was, however, less than perfect. For heavier $N > Z$ nuclei such as ^{208}Pb the calculated binding energies were deviating considerably (by more than 5 %) from the experimental values. In the present version of the model, both the isoscalar and the isovector channels of the exchange-correlation functional incorporate the additional contribution of two-pion exchange with single and double virtual $\Delta(1232)$-isobar excitations. Much better isospin properties of nuclear matter have thus been obtained. One can therefore expect improved results also for ground-state properties of $N \neq Z$ nuclei calculated with the advanced nuclear energy density functional derived the present work. This is illustrated in Fig. 3 where for the set of spherical nuclei that were used in the fit (see Tab. 2), we compare the deviations between calculated and experimental binding energies and charge radii, respectively, for the FKVW interaction with explicit inclusion of $\Delta(1232)$ excitations, and for the previous version of the interaction [12] which did not include the $\Delta(1232)$ degree of freedom. The latter displays a systematic underbinding with the increase of the neutron – proton asymmetry in heavier nuclei, and the deviations exceed 5% already for Sn isotopes. This is corrected with the additional contribution of the $\Delta(1232)$-isobar, and the new effective interaction reproduces with high accuracy the empirical masses. We also notice an improvement for the calculated charge radii (lower panel of Fig. 3), although not as dramatic as in the case of binding energies.

In this section the improved effective FKVW interaction will be tested in self-consistent calculations of ground-state observables for spherical and deformed medium-heavy and heavy nuclei. The calculations, including open-shell nuclei, are performed in the framework of the relativistic Hartree-Bogoliubov (RHB) model, a relativistic extension of the conventional Hartree-Fock-Bogoliubov

method, that provides a basis for a consistent microscopic description of ground-state properties of medium-heavy and heavy nuclei, low-energy excited states, small-amplitude vibrations, and reliable extrapolations toward the drip lines [2]. In the particle-hole channel we employ the new microscopic FKVW interaction. In comparison we also present calculations, for spherical nuclei, using the DD-ME1 interaction. The DD-ME1 model Lagrangian is characterized by a phenomenological density dependence of the σ, ω and ρ boson-nucleon vertex functions, adjusted to properties of nuclear matter and finite nuclei. The DD-ME1 effective interaction has recently been employed in a number of studies of ground-state properties of spherical and deformed nuclei [49,50], and of multipole giant resonances in spherical nuclei [51,52,53]. When compared to results obtained with standard nonlinear relativistic mean-field effective forces, the DD-ME1 interaction gives an improved description of asymmetric nuclear matter and of ground-state properties of $N \neq Z$ nuclei. In the relativistic random phase approximation (RRPA), the DD-ME1 effective interaction reproduces the experimental excitation energies of multipole giant resonances in spherical nuclei.

Pairing effects in nuclei are restricted to a narrow window of a few MeV around the Fermi level. Their scale is well separated from the scale of binding energies which are in the range of several hundred to thousand MeV. There is no empirical evidence for any relativistic effect in the nuclear pairing field. Therefore pairing can be treated as a non-relativistic phenomenon [54]. In most applications of the RHB model the pairing part of the well known and successful Gogny force [55] has been used in the particle-particle channel. We will conveniently proceed in the same way, noting at the same time that the chiral N-N potential produces very similar pairing matrix elements [56].

4.1 Spherical nuclei

In order to test the detailed isospin dependence we investigate now the systematics of isotopic chains. Deviations (in percent) of calculated binding energies from their experimental values [57] are shown in Fig. 4 for a series of even-A Sn isotopes. In addition to the FKVW interaction, computations are performed with phenomenological density-dependent interaction DD-ME1. The Gogny D1S force is used for the pairing interaction. Both with FKVW and DD-ME1, very good results are found over the entire major shell $50 \leq N \leq 82$. For the new microscopic FKVW interaction in particular, the absolute deviations of the calculated masses from data do not exceed 0.1 %. In the lower panel of Fig. 4 we display the calculated charge radii of Sn isotopes in comparison with the experimental values [58]. For both interactions the theoretical values are in excellent agreement with data.

The isotopic dependence of the deviations (in percent) between the calculated binding energies and the experimental values for even-A Pb nuclei [57], is plotted in the upper panel of Fig. 5. It is interesting to note that, although DD-ME1 and FKVW represent different physical models, they display a similar mass dependence of the calculated binding energies for the Pb isotopic chain. On a quantitative level the FKVW interaction produces better results, with the absolute deviations of the calculated masses below 0.1 % for $A \geq 190$. In lighter Pb isotopes one expects that the observed shape coexistence phenomena will have a pronounced effect on the measured masses.

Because of the intrinsic isospin independence of the effective single-nucleon spin-orbit potential, relativistic mean-field models naturally reproduce the anomalous charge isotope shifts [60]. The well known example of the anomalous kink in the charge isotope shifts of Pb isotopes is illustrated in the lower panel of Fig. 5. The results of RHB calculations with the DD-ME1 and FKVW effective interactions are shown in comparison with experimental values [61]. Both interactions reproduce in detail the A-dependence of the isotope shifts and the kink at ^{208}Pb.

The differences between the r.m.s. radii of neutron and proton ground-state distributions of Sn and Pb nuclei are shown in Fig. 6. Results obtained with the FKVW interaction are compared with data [62] for the Sn isotopes, and with the empirical value of $r_n - r_p$ in ^{208}Pb (0.20 ± 0.04 fm from proton scattering data [63], and 0.19 ± 0.09 fm from the excitation of the isovector giant dipole resonance by α-scattering [64]).

The determination of neutron density distributions provides not only basic nuclear structure information, but it also places important additional constraints on the isovector channel of the effective interactions used in nuclear models. In a recent analysis of neutron radii in non-relativistic and covariant mean-field models [65], the linear correlation between the neutron skin and the asymmetry energy was studied. In particular, it has been shown that there is a very strong linear correlation between the neutron skin thickness in ^{208}Pb and the parameters that determine the asymmetry energy. The excellent agreement between the calculated $r_n - r_p$ and the available data confirms that the isovector channel of the microscopic effective interaction FKVW is correctly represented. Note that this is achieved without ad-hoc introduction of a phenomenological ρ-meson exchange interaction.

The FKVW model is based on the framework of density functional theory and, therefore, a natural test is the comparison of the calculated density distributions with available data. In Fig. 7 we display several calculated charge form factors in comparison with data [66]. In addition to ^{48}Ca, ^{90}Zr, and ^{208}Pb, for which the charge radii i.e. the first minima of the charge form factors have been used in the fit of the parameter set FKVW (see Table 2), we

also plot the charge form factors of ^{92}Mo, ^{94}Zr, and ^{144}Sm. The theoretical charge density distributions are obtained by folding the point proton density distribution with the proton charge distribution of exponential form $\sim e^{-\Lambda r}$ (reflecting a dipole form factor), with the empirical proton charge radius. The corresponding form factors are plotted as functions of the momentum transfer $\boldsymbol{q}$:

$$F_{ch}(\boldsymbol{q}) = \frac{1}{Z}\rho_{ch}(\boldsymbol{q})\left[1 + \frac{\boldsymbol{q}^2}{8\langle P_{cm}^2\rangle} + \ldots\right] , \tag{47}$$

where $\rho_{ch}(\boldsymbol{q})$ is the Fourier transform of the spherical charge density and the second term is a center-of-mass correction. Higher-order effects in $\boldsymbol{q}^2/P_{cm}^2$ are negligible. The excellent agreement between the calculated and experimental charge form factors for momenta $|\boldsymbol{q}| \leq 2.5$ fm^{-1} demonstrates that the FKVW interaction reproduces not only the moments of the distributions, but also the detailed charge density profiles.

One of the principal advantages of using the relativistic framework lies in the fact that the effective single-nucleon spin-orbit potential arises naturally from the Dirac equation. The single-nucleon potential does not introduce any adjustable parameter for the spin-orbit interaction. In the FKVW model, in particular, the large effective spin-orbit potential in finite nuclei is generated by the strong scalar and vector condensate background fields of about equal magnitude and opposite sign, induced by changes of the QCD vacuum in the presence of baryonic matter [12]. In Fig. 8 we plot the deviations (in percent) between the calculated and experimental values of the energy spacings between spin-orbit partner-states in a series of doubly closed-shell nuclei. Even though the Kohn-Sham orbitals cannot be directly identified with the single-nucleon states in the interacting system, the calculated energy spacings between spin-orbit partners, especially the ones close to the Fermi surface, compare well with the experimental values. The experimental data are from Ref. [67], and the theoretical spin-orbit splittings have been calculated with the FKVW and DD-ME1 interactions. For the phenomenological DD-ME1 interaction the large scalar and vector nucleon self-energies which generate the spin-orbit potential, arise from the exchange of "sigma" and "omega" bosons with adjustable strength parameters. We notice that, even though the values calculated with DD-ME1 are already in very good agreement with experimental data, a further improvement is obtained with the FKVW interaction. This remarkable agreement indicates that the initial estimates Eqs. (37) and (38) for the condensate background couplings have perhaps been more realistic than anticipated, considering the uncertainties of lowest-order in-medium QCD sum rules.

4.2 Deformed nuclei

Deformed nuclei with $N > Z$ present further important tests for nuclear structure models. Ground-state properties, in particular, are sensitive to the isovector channel of the effective interaction, to the spin-orbit term of the effective single-nucleon potentials and to the effective mass.

In this section we test our advanced model in the region $60 \leq Z \leq 80$. We compare predictions of the RHB calculations for the total binding energies, charge radii and ground-states quadrupole deformations of nine even-Z isotopic chains with available data. The FKVW effective interaction is used in the particle-hole channel, and pairing correlations are described by the pairing part of the finite range Gogny D1S interaction [55].

The deviations (in percent) of the calculated binding energies from the experimental data [57] for Nd, Sm, Gd, Dy, Er, Yb, Hf, W, and Os isotopes are plotted in Fig. 9. Good agreement is found over the entire region of deformed nuclei. The maximum deviation of the calculated binding energies from data is below 0.5% for all isotopes.

In Fig. 10 we compare the calculated charge radii with data from Ref. [58]. The charge density is constructed by folding the calculated (point) proton density distribution with the empirical proton-charge distribution. The calculation of the charge rms radius from the full charge form factor is quite involved for deformed nuclei [1,59]. We employ the frequently used simplified expression

$$r_c = \sqrt{r_p^2 + 0.64 \text{ fm}^2} \,, \tag{48}$$

where r_p^2 is the nuclear mean-square radius of the (point) proton density distribution. The calculated charge radii reproduce in detail the experimental isotopic trends.

The ground-state quadrupole deformation parameter β_2, proportional to the expectation value of the quadrupole operator $\langle\phi_0|3z^2-r^2|\phi_0\rangle$, is calculated according to the prescription of Ref. [68]. The theoretical values of the quadrupole deformation parameter are displayed in Fig. 11, in comparison with the empirical data extracted from $B(E2)$ transitions [69]. We notice that the RHB results reproduce not only the global trend of the data but also the saturation of quadrupole deformations for heavier isotopes.

The structure of nuclei far from stability provides a particularly important testing ground for global effective interactions. An interesting question, therefore, is how far from stability can we extrapolate the predictions of the FKVW interaction. While an extensive analysis of this problem is beyond the scope

of the present work, we consider in detail the example of neutron-deficient Pb isotopes which exhibit an interesting variety of coexisting shapes. They are characterized by the competition of low-lying prolate and oblate minima. Recent data [70] on energy spectra and charge radii indicate that, although the ground states of neutron-deficient Pb nuclei are spherical, both oblate (two-particle – two-hole proton excitations across the $Z = 82$ major shell) and prolate (four-particle – four-hole proton excitations) low-lying minima can be observed for $N < 110$ at almost identical excitation energies.

A number of theoretical analyses of shell quenching and shape coexistence phenomena in neutron-deficient Hg, Pb and Po nuclei has been reported in recent years. The quantitative description of coexisting spherical, oblate and prolate minima necessitates restoration of broken symmetries and the explicit treatment of quadrupole fluctuations. In particular, excellent results for shape coexistence in neutron-deficient Pb isotopes have recently been obtained by performing configuration mixing of angular momentum projected self-consistent mean-field states, calculated with the finite range and density dependent Gogny interaction [71], and with the Skyrme interaction SLy6 supplemented by a density-dependent zero-range pairing force [72].

The model employed in the present work does not include angular momentum projection, nor can it account for configuration mixing effects. Nevertheless, we can compare the potential energy curves, calculated as functions of the axial quadrupole deformation, with the corresponding mean-field energy curves calculated with the Gogny [71] and Skyrme [72] interactions.

In Fig. 12 we display the calculated binding energy curves of even-A $^{182-196}Pb$ isotopes as functions of the quadrupole deformation. The curves correspond to axially deformed RHB model solutions with constrained quadrupole deformation. The effective interaction is FKVW + Gogny D1S (pairing). The general agreement with the mean-field potential energy curves of Refs.[71] and [72] is satisfactory and, in particular, the present calculation predicts the coexistence of oblate and prolate minima at almost identical excitation energies in $^{186,188}Pb$, in agreement with data. The relative excitation energies of coexisting minima based on different intruder configurations are determined by the spherical magic and semi-magic energy gaps. For $A \geq 190$ the minimum on the prolate side vanishes, in accordance with the nonrelativistic calculations performed with the Gogny and Skyrme-SLy6 interactions. In these nuclei, however, we also calculate a tiny shift of the ground-state minimum toward prolate deformation, a result not predicted by the two non-relativistic interactions, and not corroborated by available data. Although the quantitative analysis of the structure of neutron-deficient Pb nuclei must include additional correlations related to the restoration of broken symmetries and quadrupole fluctuations, it is indeed an encouraging result that the FKVW interaction reproduces the isotopic trend of the coexistence of shapes in heavy

nuclei far from stability. This reinforces the confidence in the detailed behavior of the isospin-dependent interaction derived from chiral two-pion exchange dynamics, improved by explicit $\Delta(1232)$ components.

5 Summary, conclusions and further comments

We have derived a relativistic nuclear energy density functional with connections to two closely linked features of QCD in the low-energy limit:
a) in-medium changes of vacuum condensates;
b) spontaneous chiral symmetry breaking.

The leading changes of the chiral (quark) condensate and quark density in the presence of baryonic matter are sources of strong (attractive) scalar and (repulsive) vector fields experienced by nucleons in the nucleus. These fields produce Hartree potentials of about 0.35 GeV in magnitude at nuclear matter density, in accordance with QCD sum rules. While these scalar and vector potentials cancel approximately in their contribution to the energy, they are at the origin of the large spin-orbit splitting in nuclei.

The spontaneously broken chiral symmetry in QCD introduces pions as Goldstone bosons with well-defined (derivative) couplings to baryons plus symmetry breaking corrections. In the present approach the exchange-correlation part of the energy density functional is deduced from the long- and intermediate-range interactions generated by one- and two-pion exchange processes. They have been computed using in-medium chiral perturbation theory with explicit inclusion of $\Delta(1232)$ degrees of freedom which turn out to be important. Regularization dependent contributions to the energy density, calculated at three-loop level, are absorbed in contact interactions with constants representing unresolved short-distance dynamics.

This framework is translated into a point-coupling model with density-dependent interaction vertices. This is done for the practical purpose of deriving and solving self-consistent Dirac equations (relativistic analogues of Kohn-Sham equations) in order to determine the nucleon densities which enter the energy functional. We demonstrate that this scheme works extremely well when confronted with a large number of high-precision nuclear data over a broad range of spherical and deformed nuclei. In fact the quantitative accuracy of the calculated binding energies and radii is such that deviations from empirical data are generally less than 0.5% throughout the nuclear chart and usually much less (0.1%) for medium-heavy nuclei. It has to be noted, however, that these results still do not reach the accuracy of the best phenomenological mass tables (recent trends in the determination of nuclear masses have been reviewed in Ref. [73]). Modern Skyrme-based microscopic mass formulas, with a total

of ≈ 20 empirical parameters, fit the measured masses of more than two thousand nuclei with an rms error of less than 700 keV. In addition, they also produce excellent results for charge radii, with an rms deviation of ≈ 0.025 fm for the absolute charge radii and charge isotope shifts of more than 500 nuclei. The nuclear energy density functional developed in this work is not, of course, a mass formula and, with only a small set of adjustable parameters, is not designed to compete with such a level of accuracy. Nevertheless, it provides an excellent microscopic framework on which a more fundamental approach to the calculation of nuclear masses can be based.

A special focus in this work is on systematic studies along isotopic chains. Binding energies, as well as proton and neutron radii of such systems, with fixed number of protons but varying number of neutrons, are an excellent testing ground for the detailed isospin properties of the effective interaction. The quality of the results points to the fact that chiral pion dynamics, and especially the Van der Waals-like two-pion exchange forces with inclusion of the $\Delta(1232)$, is capable of generating the proper isospin dependence required by observables in isotopic sequences.

The construction of the density functional involves an expansion of nucleon self-energies in powers of the Fermi momentum up to and including terms of order k_f^6, or equivalently, $O(\rho^2)$ in the proton and neutron densities. Up to this order the present model has seven parameters, four of which are related to contact (counter) terms that appear in the chiral perturbation theory treatment of nuclear matter. One parameter fixes a surface (derivative) term and two more represent the strengths of scalar and vector Hartree fields.

In the "best fit" set which reproduces a large amount of data on nuclear ground state properties, five of those seven parameters turn out to be surprisingly close to estimates and predictions from in-medium QCD sum rules and ChPT calculations for nuclear matter. In particular, the strong scalar and vector (Hartree) fields required to reproduce spin-orbit splittings are remarkably compatible with the leading-order QCD sum rule estimates. The fitted coefficient b_3 multiplying the $O(k_f^3)$ term in the chiral expansion of the nucleon self-energy, is within less than 5 % of the one from the ChPT calculation for nuclear matter. For the corresponding coefficient a_3 in the expansion of the isospin dependent nucleon self-energy, the deviation (between fit to the nuclear data base and ChPT evaluation of the symmetry energy) is even less than 2 %. The surface term required to reproduce the detailed systematics of nuclear radii is within less than 10 % of the ChPT prediction for slightly inhomogeneous nuclear matter. This prediction is actually parameter-free since the corresponding loop integrals involve only finite, regularization independent pieces. The exceptions that deviate from this overall pattern are the two parameters related to the three-body contact interaction terms (of order k_f^6, or ρ^2, in the self-energies) for which the nuclear data require more attraction

than anticipated by the in-medium ChPT estimate. On absolute scales, however, these three-body terms are relatively small within the hierarchy of the k_f expansion: an encouraging result although it cannot strictly be taken as proof of convergence.

In this work we have only considered the low-energy QCD constraints on the effective interaction in the particle-hole channel, whereas the pairing part of the Gogny D1S force has been used for the effective interaction in the particle-particle channel. One could, of course, extend the chiral EFT approach to the pairing channel, and this would introduce additional contact terms. The first step in this direction has been taken in Ref. [56], where an improved version of the chiral nucleon-nucleon potential at next-to-next-to-leading order has been used to calculate the $^1S_0$ pairing gap in isospin-symmetric nuclear matter. The pairing potential consists of long-range one- and two-pion exchange terms, and two NN-contact couplings. It has been shown that the inclusion of the two-pion exchange at the next-to-next-to-leading order reduces substantially the cut-off dependence of the $^1S_0$ pairing gap, indicating reasonable convergence of the small momentum expansion. The results are very close to those obtained with the phenomenological Gogny D1S force.

The exchange-correlation energy functional in nuclear matter, calculated by in-medium chiral perturbation theory, has been used in Kohn-Sham calculations of finite nuclei by employing a second-order gradient correction to the local density approximation. Even though the quality of the results is on the level of the best phenomenological (non-relativistic and relativistic) self-consistent mean-field models, obviously the goal is to further improve the accuracy of the calculated nuclear ground-state energies and density distributions all over the periodic table. In the next step this will require the development of an accurate generalized gradient approximation for the nuclear exchange-correlation energy.

An important issue will also be the relation with the universal low-momentum interaction V_{low-k} [74], deduced from phase-shift equivalent nucleon-nucleon interactions. An apparent close correspondence between perturbative in-medium chiral dynamics and V_{low-k} in the low-density limit has already been pointed out recently in Ref. [17]. This is a non-trivial observation, given that the input to the chiral approach [17] has been fixed to nuclear matter properties and not to NN phase shifts. The applicability of a perturbative expansion scheme for nuclear matter with low-momentum interactions, which is the basic hypothesis behind our approach, is discussed in Ref. [75]. Further studies towards foundations along these lines are presently being pursued.

This work has demonstrated that chiral effective field theory provides a consistent microscopic framework in which both the isoscalar and isovector channels of a universal nuclear energy density functional can be formulated. The

present approach to nuclear DFT establishes a fundamental link between low-energy QCD and ground-state properties of finite nuclei. From a practical point of view, a fully microscopic basis of effective nuclear interactions is especially important for studies of nuclear structure in regions far from the valley of β-stability, where extrapolations of phenomenological (non-relativistic and relativistic) models lack predictive power.

6 Acknowledgments

Helpful discussions with Stefan Fritsch, Tamara Nikšić and Peter Ring are gratefully acknowledged. One of the authors (W.W.) thanks Tony Thomas, the Theory Group at Jefferson Lab, and ECT* in Trento for their hospitality during the preparation of this paper.

7 Appendix

Here we present details of the nucleon self-energies from in-medium chiral perturbation theory and their translation into a point-coupling model with density-dependent vertices. In [13,14,17] the momentum and density-dependent single particle potential of nucleons in asymmetric nuclear matter:

$$U(p,k_f) - U_I(p,k_f)\tau_3\delta + \mathcal{O}(\delta^2) \quad \text{with} \quad \delta = \frac{\rho^n - \rho^p}{\rho^n + \rho^p} \,, \tag{49}$$

has been calculated within two-loop in-medium chiral perturbation theory (ChPT).

From the sums

$$\begin{aligned} U(p=k_f,k_f) &= \Sigma_S^{\rm ChPT}(k_f,\rho) + \Sigma_V^{\rm ChPT}(k_f,\rho) \\ -U_I(p=k_f,k_f)\delta &= \Sigma_{TS}^{\rm ChPT}(k_f,\rho) + \Sigma_{TV}^{\rm ChPT}(k_f,\rho) \end{aligned} \tag{50}$$

of the scalar and vector nucleon self-energies in the isoscalar and isovector channels can be extracted at the Fermi surface, $p = k_f$. It has been shown that the differences between scalar and vector parts of the ChPT self-energies are very small (suppressed by factors M_N^{-2}) and linearly proportional to ρ. Their effects can therefore be absorbed as small corrections to the condensate

fields. This motivates the following ansatz:

$$\begin{cases} \Sigma_S^{\rm ChPT}(k_f,\rho) = \frac{1}{2}U(k_f,k_f) \\ \Sigma_V^{\rm ChPT}(k_f,\rho) = \frac{1}{2}U(k_f,k_f) \\ \Sigma_{TS}^{\rm ChPT}(k_f,\rho) = -\frac{1}{2}U_I(k_f,k_f)\delta \\ \Sigma_{TV}^{\rm ChPT}(k_f,\rho) = -\frac{1}{2}U_I(k_f,k_f)\delta \end{cases} , \tag{51}$$

in which the single-nucleon self-energy Eq. (50) is equally divided between the vector Eq. (26) and the scalar Eq. (28) components. For the ChPT isoscalar and isovector self-energies [17] a polynomial fit up to order k_f^6 is performed:

$$\begin{aligned} U(k_f;b_3,b_5,b_6) = & \ [c_3+2b_3]\,\frac{k_f^3}{\Lambda^2} + c_4\,\frac{k_f^4}{\Lambda^3} + \left[c_5+\frac{8}{3}b_5\right]\frac{k_f^5}{\Lambda^4} \\ & + \ [c_6+3b_6]\,\frac{k_f^6}{\Lambda^5} + \mathcal{O}(k_f^7) \end{aligned} \tag{52}$$

and

$$\begin{aligned} U_I(k_f,a_3,a_5,a_6,b_5) = & \ [d_3+2a_3]\,\frac{k_f^3}{\Lambda^2} \\ & + \ d_4\,\frac{k_f^4}{\Lambda^3} + \left[d_5+2a_5-\frac{10}{9}b_5\right]\frac{k_f^5}{\Lambda^4} \\ & + \ [d_6+2a_6]\,\frac{k_f^6}{\Lambda^5} + \mathcal{O}(k_f^7)\ , \end{aligned} \tag{53}$$

where b_i and a_i are the dimensionless short-distance regularization constants appearing in the counter terms (39) and (40). They subsume all unresolved short-range two- and three-body dynamics, plus possible higher order (four-loop etc.) effects not evaluated but contributing already at order k_f^6. The constants c_i and d_i are derived directly from the in-medium ChPT calculations of the finite (regularization-independent) parts of one- and two-pion-exchange contributions to the energy, with inclusion of $\Delta(1232)$ intermediate states. They are taken over unchanged from Ref. [17]. Note that the coupling strengths g_i in the isoscalar single-particle potential (45) are identified as

$$\begin{aligned} g_3 &= c_3 + 2b_3\ . \\ g_4 &= c_4\ , \\ g_5 &= c_5 + \frac{8}{5}b_5\ , \\ g_6 &= c_6 + 3b_6\ . \end{aligned} \tag{54}$$

The counter term constants b_i and a_i are listed in Table 3. The constants c_i and d_i are collected in Table 5 at the reference scale $\Lambda = 2\pi f_\pi \simeq 0.58$ GeV.

In order to determine the density-dependent couplings of the exchange correlation pieces generated by the point-coupling model, the ChPT self-energies are first re-expressed in terms of the baryon density $\rho = 2k_f^3/3\pi^2 = \rho^p + \rho^n$ and the isovector density $\rho_3 = \rho^p - \rho^n$:

$$\Sigma_S^{\rm ChPT}(k_f,\rho) = \left(c_{s1} + c_{s2}\rho^{\frac{1}{3}} + c_{s3}\rho^{\frac{2}{3}} + c_{s4}\rho\right)\rho \ , \tag{55}$$

$$\Sigma_V^{\rm ChPT}(k_f,\rho) = \left(c_{v1} + c_{v2}\rho^{\frac{1}{3}} + c_{v3}\rho^{\frac{2}{3}} + c_{v4}\rho\right)\rho \ , \tag{56}$$

$$\Sigma_{TS}^{\rm ChPT}(k_f,\rho) = \left(c_{ts1} + c_{ts2}\rho^{\frac{1}{3}} + c_{ts3}\rho^{\frac{2}{3}} + c_{ts4}\rho\right)\rho_3 \ , \tag{57}$$

$$\Sigma_{TV}^{\rm ChPT}(k_f,\rho) = \left(c_{tv1} + c_{tv2}\rho^{\frac{1}{3}} + c_{tv3}\rho^{\frac{2}{3}} + c_{tv4}\rho\right)\rho_3 \ , \tag{58}$$

Next these self-energies are identified with the corresponding contributions to the potentials in the point coupling single-nucleon Dirac equation (26)-(30):

$$\Sigma_S^{\rm PC}(k_f,\rho) = G_S^{(\pi)}(\rho)\,\rho_S \ , \tag{59}$$

$$\Sigma_V^{\rm PC}(k_f,\rho) = G_V^{(\pi)}(\rho)\,\rho + \frac{1}{2}\left\{\frac{\partial G_V^{(\pi)}(\rho)}{\partial\rho}\rho^2 + \frac{\partial G_S^{(\pi)}(\rho)}{\partial\rho}\rho_S^2\right\} \ , \tag{60}$$

$$\Sigma_{TS}^{\rm PC}(k_f,\rho) = G_{TS}^{(\pi)}(\rho)\,\rho_{S3} \ , \tag{61}$$

$$\Sigma_{TV}^{\rm PC}(k_f,\rho) = G_{TV}^{(\pi)}(\rho)\,\rho_3 \ , \tag{62}$$

The resulting expressions for the density-dependent couplings of the pionic fluctuation terms read [2]

$$G_S^{(\pi)}(\rho) = c_{s1} + c_{s2}\rho^{\frac{1}{3}} + c_{s3}\rho^{\frac{2}{3}} + c_{s4}\rho \ , \tag{63}$$

$$G_V^{(\pi)}(\rho) = \bar{\mathbf{c}}_{\mathbf{v1}} + \bar{\mathbf{c}}_{\mathbf{v2}}\rho^{\frac{1}{3}} + \bar{\mathbf{c}}_{\mathbf{v3}}\rho^{\frac{2}{3}} + \bar{\mathbf{c}}_{\mathbf{v4}}\rho \ , \tag{64}$$

$$G_{TS}^{(\pi)}(\rho) = c_{ts1} + c_{ts2}\rho^{\frac{1}{3}} + c_{ts3}\rho^{\frac{2}{3}} + c_{ts4}\rho \ , \tag{65}$$

$$G_{TV}^{(\pi)}(\rho) = c_{tv1} + c_{tv2}\rho^{\frac{1}{3}} + c_{tv3}\rho^{\frac{2}{3}} + c_{tV4}\rho \ , \tag{66}$$

where the inclusion of the rearrangement term Σ_R^0 redefines the isoscalar-vector coefficients:

$$\begin{cases} \bar{\mathbf{c}}_{\mathbf{v1}} = c_{v1} \\ \bar{\mathbf{c}}_{\mathbf{v2}} = \frac{1}{7}(6c_{v2} - c_{s2}) \\ \bar{\mathbf{c}}_{\mathbf{v3}} = \frac{1}{4}(3c_{v3} - c_{s3}) \\ \bar{\mathbf{c}}_{\mathbf{v4}} = \frac{1}{3}(2c_{v4} - c_{s4}) \ . \end{cases} \tag{67}$$

[2] small differences between ρ and ρ_S at nuclear matter densities are neglected here.

Table 5
Coefficients of the expansions (52-53) up to order k_f^6 in the isoscalar and isovector channel. The reference scale is $\Lambda = 2\pi f_\pi \simeq 0.58$ GeV.

c_3	3.01	d_3	-2.80
c_4	2.67	d_4	-0.35
c_5	2.17	d_5	-8.88
c_6	13.70	d_6	11.50

Table 6
Coefficients of the expansion of the density-dependent couplings (63) – (66) in powers of the baryon density. The input parameters in this example are those of the ChPT calculation [17] ($b_3 = -3.05, a_3 = 2.16, b_5 = a_5 = 0, b_6 = -a_6 = 2.82$).

$c_{s1} = c_{v1}$	-2.65 fm^2	$c_{ts1} = c_{tv1}$	1.31 fm^2	$\bar{\mathbf{c}}_{\mathbf{v1}}$	-2.65 fm^2
$c_{s2} = c_{v2}$	1.91 fm^3	$c_{ts2} = c_{tv2}$	-0.25 fm^3	$\bar{\mathbf{c}}_{\mathbf{v2}}$	1.36 fm^3
$c_{s3} = c_{v3}$	1.29 fm^4	$c_{ts3} = c_{tv3}$	-5.29 fm^4	$\bar{\mathbf{c}}_{\mathbf{v3}}$	0.65 fm^4
$c_{s4} = c_{v4}$	2.59 fm^5	$c_{ts4} = c_{tv4}$	6.65 fm^5	$\bar{\mathbf{c}}_{\mathbf{v4}}$	0.43 fm^5

The coefficients of the expansion of the density-dependent couplings in powers of the baryon density (Eqs. (63) – (67)) are listed in Table 6.

References

[1] M. Bender, P.-H. Heenen, and P.-G. Reinhard, Rev. Mod. Phys. **75** (2003) 121.

[2] D. Vretenar, A.V. Afanasjev, G.A. Lalazissis, and P. Ring, Phys. Rep. **409** (2005) 101.

[3] P. Hohenberg and W. Kohn, Phys. Rev. B**136** (1964) 864.

[4] W. Kohn and L. J. Sham, Phys. Rev. A**140** (1965) 1133.

[5] W. Kohn, Rev. Mod. Phys. **71**, (1999) 1253.

[6] R. M. Dreizler and E. K. U. Gross, Density Functional theory, Spinger-Verlag, 1990.

[7] G. A. Lalazissis, P. Ring, and D. Vretenar (Eds.), Extended Density Functionals in Nuclear Structure Physics, Lecture Notes in Physics **641**, Springer, Heidelberg, 2004.

[8] S. J. Puglia, A Bhattacharyya, and R. J. Furnstahl, Nucl. Phys. A**723** (2003) 145.

[9] A Bhattacharyya and R. J. Furnstahl, Nucl. Phys. A**747** (2005) 268.

[10] R. J. Furnstahl, J. Phys. G**31** (2005) S1357 [arXiv:nucl-th/0412093].

[11] P. Finelli, N. Kaiser, D. Vretenar and W. Weise, Eur. Phys. J. A**17** (2003) 573 [arXiv:nucl-th/0205016].

[12] P. Finelli, N. Kaiser, D. Vretenar and W. Weise, Nucl. Phys. A**735** (2004) 449 [arXiv:nucl-th/0307069].

[13] N. Kaiser, S. Fritsch and W. Weise, Nucl. Phys. A**697** (2002) 255 [arXiv:nucl-th/0105057].

[14] N. Kaiser, S. Fritsch and W. Weise, Nucl. Phys. A**700** (2002) 343 [arXiv:nucl-th/0108010].

[15] S. Fritsch and N. Kaiser, Eur. Phys. J. A**17** (2003) 11 [arXiv:nucl-th/0207057].

[16] N. Kaiser, S. Fritsch and W. Weise, Nucl. Phys. A**724** (2003) 47 [arXiv:nucl-th/0212049].

[17] S. Fritsch, N. Kaiser and W. Weise, Nucl. Phys. A**750** (2005) 259 [arXiv:nucl-th/0406038].

[18] D.G. Madland, B.A. Nikolaus and T. Hoch, Phys. Rev. C**46** (1992) 1757.

[19] J. J. Rusnak and R. J. Furnstahl, Nucl. Phys. A**627** (1997) 495 [arXiv:nucl-th/9708040].

[20] T. Burvenich, D. G. Madland, J. A. Maruhn and P. G. Reinhard, Phys. Rev. C**65** (2001) 044308 [arXiv:nucl-th/0111012].

[21] E. Epelbaum, Prog. Part. Nucl. Phys. (accepted for publication) [arXiv:nucl-th/0509032].

[22] N. Kaiser, Phys. Rev. C**70** (2004) 034307 [arXiv:nucl-th/0407116].

[23] R. J. Furnstahl and B. D. Serot, Nucl. Phys. A**671** (2000) 447 [arXiv:nucl-th/9911019].

[24] R. M. Dreizler, Lect. Notes Phys. **620** (2003) 123.

[25] C. Speicher, R. M. Dreizler and E. Engel, Ann. Phys. (N.Y.) **213** (1992) 312.

[26] R. N. Schmid, E. Engel and R. M. Dreizler, Phys. Rev. C**52** (1995) 164.

[27] B. D. Serot and J. D. Walecka, Adv. Nucl. Phys. **16** (1986) 1; P. Ring, Prog. Part. Nucl. Phys. **37** (1996) 193; B. D. Serot and J. D. Walecka, Int. J. Mod. Phys. E**6** (1997) 515 [arXiv:nucl-th/9701058].

[28] P. Ring, Lect. Notes Phys. **641** (2004) 175.

[29] R. J. Furnstahl, Lect. Notes Phys. **641** (2004) 1 [arXiv:nucl-th/0307111].

[30] C. Fuchs, H. Lenske, and H.H. Wolter, Phys. Rev. C**52** (1995) 3043 [arXiv:nucl-th/9507044].

[31] H. Lenske, Lect. Notes Phys. **641** (2004) 147, and references therein.

[32] S. Typel and H.H. Wolter, Nucl. Phys. A**656** (1999) 331.

[33] N. M. Hugenholtz and L. Van Hove, Physica **24** (1958) 363.

[34] B. L. Ioffe, Phys. At. Nucl. (Yad. Fiz.) **66** (2003) 30 [arXiv:hep-ph/0207191] and refs. therein.

[35] T. D. Cohen, R. J. Furnstahl and D. K. Griegel, Phys. Rev. Lett. **67** (1991) 961.

[36] R. J. Furnstahl, D. K. Griegel and T. D. Cohen, Phys. Rev. C**46** (1992) 1507.

[37] T. D. Cohen, R. J. Furnstahl, D. K. Griegel and X. m. Jin, Prog. Part. Nucl. Phys. **35** (1995) 221 [arXiv:hep-ph/9503315].

[38] E.G. Drukarev and E.M. Levin, Nucl. Phys. A**511** (1990) 679.

[39] E.G. Drukarev and E.M. Levin, Prog. Part. Nucl. Phys. **27** (1991) 77.

[40] B. L. Ioffe, Nucl. Phys. B**188** (1981) 317.

[41] A. Akmal, V. R. Pandharipande and D. G. Ravenhall, Phys. Rev. C**58** (1998) 1804 [arXiv:nucl-th/9804027].

[42] G. Q. Li, R. Machleidt and R. Brockmann, Phys. Rev. C**45** (1992) 2782.

[43] J. W. Negele and D. Vautherin, Phys. Rev. C**5** (1972) 1472.

[44] D. Vautherin and D. M. Brink, Phys. Rev. C**5** (1972) 626.

[45] L. N. Savushkin and H. Toki, "The Atomic Nucleus as Relativistic System", Springer-Verlag 2004, and references therein.

[46] M. Bender, K. Rutz, P. G. Reinhard and J. A. Maruhn, Eur. Phys. J. A**7** (2000) 467 [arXiv:nucl-th/9910025].

[47] P. Moller, J. R. Nix, W. D. Myers and W. J. Swiatecki, Atom. Data Nucl. Data Tabl. **59** (1995) 185 [arXiv:nucl-th/9308022].

[48] G. A. Lalazissis, J. Konig and P. Ring Phys. Rev. C**55** (1997) 540 [arXiv:nucl-th/9607039].

[49] T. Nikšić, D. Vretenar, P. Finelli and P. Ring, Phys. Rev. C**66** (2002) 024306 [arXiv:nucl-th/0205009].

[50] T. Nikšić, D. Vretenar, G. A. Lalazissis, and P. Ring, Phys. Rev. C**69** (2004) 047301.

[51] T. Nikšić, D. Vretenar, and P. Ring, Phys. Rev. C**66** (2002) 064302.

[52] D. Vretenar, T. Nikšić, and P. Ring, Phys. Rev. C**68** (2003) 024310.

[53] N. Paar, T. Nikšić, D. Vretenar, and P. Ring, Phys. Rev. C**69** (2004) 054303 [nucl-th/0402094].

[54] M. Serra, A. Rummel and P. Ring, Phys. Rev. C**65** (2001) 014304.

[55] J.F. Berger, M. Girod, and D. Gogny, Nucl. Phys. A**428** (1984) 23c;J. F. Berger, M. Girod, and D. Gogny, Commput. Phys. Commun. **63** (1991) 365.

[56] N. Kaiser, T. Niksic and D. Vretenar, Eur. Phys. J. A**25** (2005) 257 [arXiv:nucl-th/0411038].

[57] G.Audi, A.H.Wapstra and C.Thibault, Nuc. Phys. A**729** (2003) 337.

[58] E.G. Nadjakov, K.P. Marinova, and Yu.P. Gangrsky, At. Data Nucl. Data Tables **56** (1994) 133.

[59] W. Bertozzi, J. Friar, J. Heisenberg and J. W. Negele, Phys. Lett. B**41** (1972) 408.

[60] M.M. Sharma, G.A. Lalazissis, and P. Ring, Phys. Lett. B**317** (1993) 9 [nucl-th/9310009].

[61] P. Aufmuth, K. Heilig, and A. Steudel, At. Data Nucl. Data Tables **37** (1987) 462.

[62] A. Krasznahorkay *et al.*, Phys. Rev. Lett. **82** (1999) 3216.

[63] V.E. Starodubsky and N.M. Hintz, Phys. Rev. C**49** (1994) 2118.

[64] A. Krasznahorkay *et al.*, Nucl. Phys. A**567**, (1994) 521.

[65] R.J. Furnstahl, Nucl. Phys. A**706** (2002) 85 [arXiv:nucl-th/0112085].

[66] H. de Vries, C.W. de Jager, and C. de Vries, At. Data Nucl. Data Tables **36** (1987) 495.

[67] NUDAT database, National Nuclear Data Center, [http://www.nndc.bnl.gov/nndc/nudat/]

[68] J. Libert and P. Quentin, Phys. Rev. C**25** (1982) 571.

[69] S. Raman, C. Nestor, and P. Tikkanen, At. Data Nucl. Data Tables **78** (2001) 1.

[70] RA. N. Andreyev *et al.*, Nature **405** (2000) 430; A. N. Andreyev *et al.*, Nucl. Phys. A**682** (2001) 482c; Julin, K. Helariutta and M. Muikku, J. Phys. G**27** (2001) R109.

[71] R. R. Rodríguez-Guzmán, J. L. Egido, and L. M. Robledo, Phys. Rev. C **69** (2004) 054319.

[72] T. Duguet, M. Bender, P. Bonche and P. H. Heenen, Phys. Lett. B **559** (2003) 201 [arXiv:nucl-th/0212016]; M. Bender, P. Bonche, T. Duguet and P. H. Heenen, Phys. Rev. C **69** (2004) 064303 [arXiv:nucl-th/0311090].

[73] D. Lunney, J. M. Pearson, and C. Thibault, Rev. Mod. Phys. **75** (2003) 1021.

[74] S.K Bogner, T.T.S. Kuo and A. Schwenk, Phys. Reports **386** (2003) 1.

[75] S.K Bogner, A. Schwenk, R.J. Furnstahl and A. Nogga, Nucl. Phys. A**763** (2005) 59 [arXiv:nucl-th/0504043].

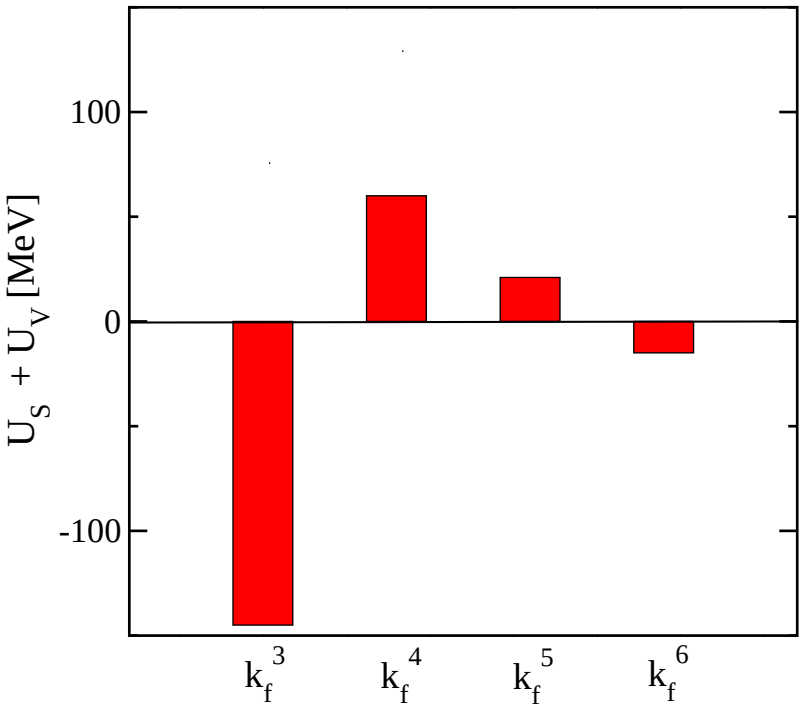

Fig. 1. Coefficients U_n in the expansion (46) of the nuclear single particle potential in fractional powers $n/3$ of the density $\rho(\mathbf{r})$ for the case of a density $\rho \simeq \rho_{sat}$.

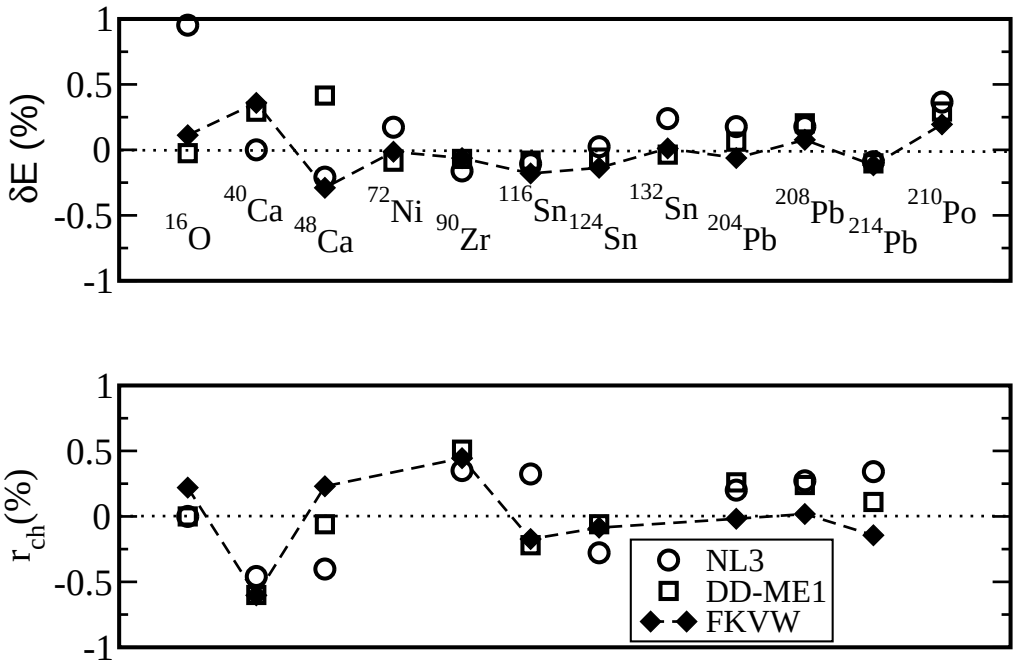

Fig. 2. Deviations (in percent) of the calculated binding energies (upper panel) and charge radii (lower panel) from the experimental values [57,58], for three relativistic effective interactions: the non-linear meson-exchange NL3 [48] (circles), the density-dependent meson-exchange DD-ME1 [49] (squares), and the microscopic density-dependent point-coupling interaction FKVW (diamonds). The calculations are performed in the RMF+BCS model with empirical gaps [47].

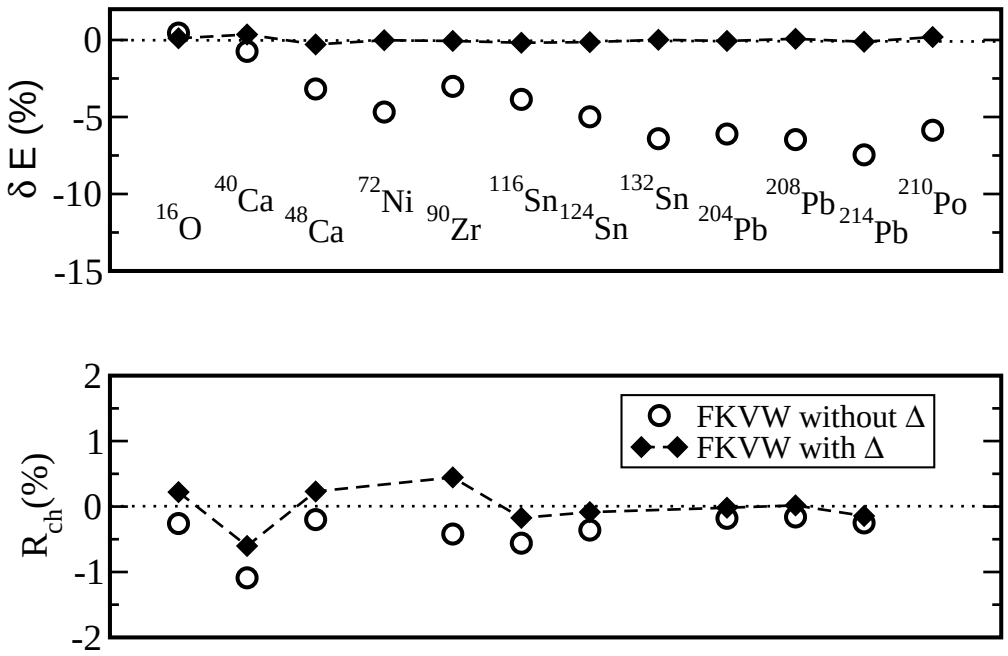

Fig. 3. Deviations (in percent) of the calculated binding energies (upper panel) and charge radii (lower panel) from the experimental values [57,58] for the density-dependent point-coupling interaction FKVW with explicit inclusion of $\Delta(1232)$ excitations (diamonds) used in the present work, and for the previous version [12] which did not include the $\Delta(1232)$ degree of freedom (cirles).

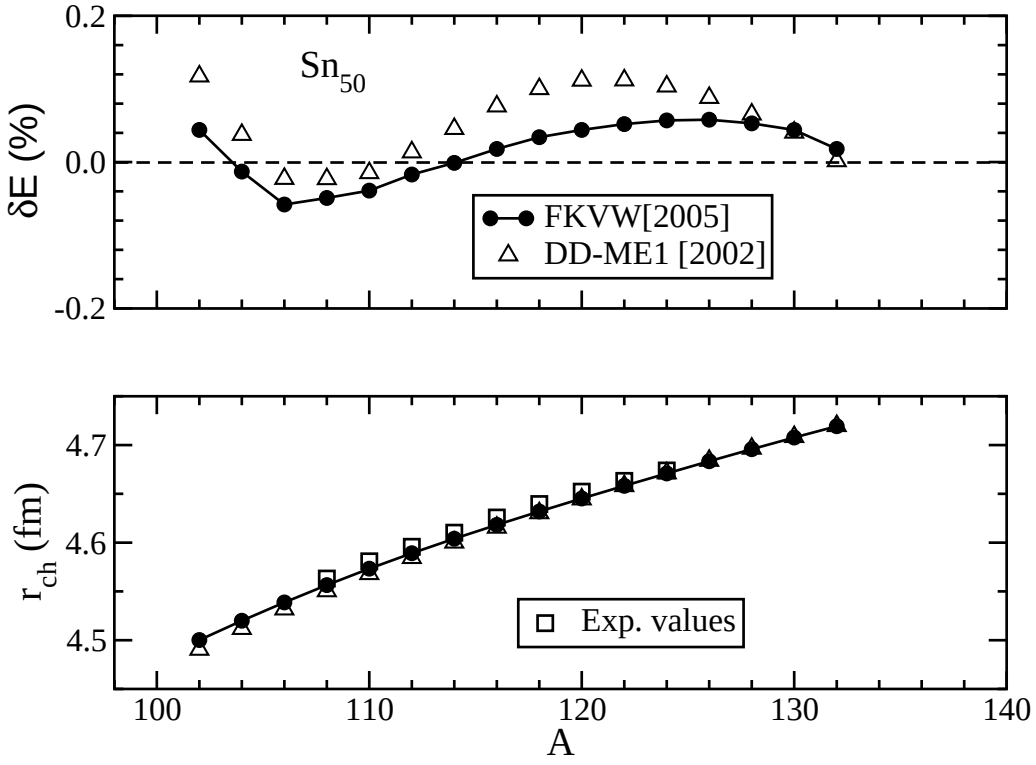

Fig. 4. The deviations (in percent) of the calculated binding energies from the experimental values (upper panel) [57], and the calculated charge radii in comparison with data [58], for the chain of even-A *Sn* isotopes. The theoretical values are calculated in the RHB model with the DD-ME1 [49] (triangles) and FKVW (dots) density-dependent effective interactions, and with the Gogny interaction in the pairing channel.

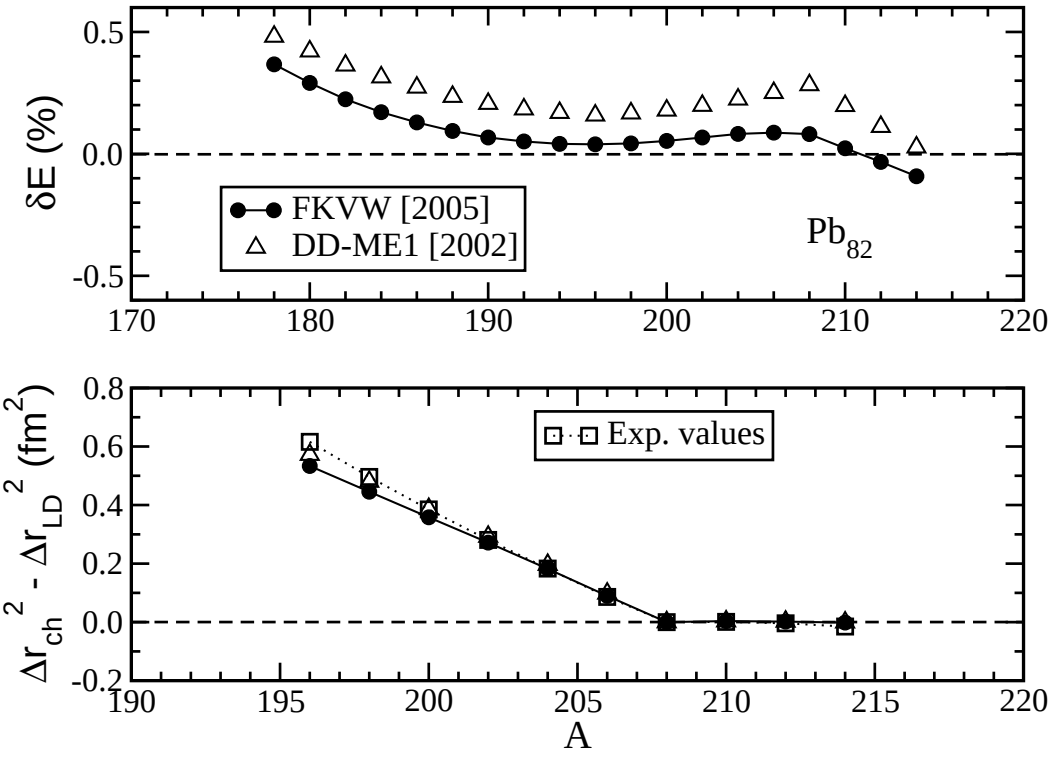

Fig. 5. The deviations (in percent) of the calculated binding energies from the experimental values (upper panel) [57], and the calculated charge isotope shifts in comparison with data [61], for the chain of even-A Pb isotopes. The charge isotope shifts are defined: $\Delta r^2_{ch} = r^2_{ch}(A) - r^2_{ch}(^{208}Pb)$ and $\Delta r^2_{LD} = r^2_{LD}(A) - r^2_{LD}(^{208}Pb)$, where the liquid-drop estimate is $r^2_{LD}(A) = \frac{3}{5} r_0^2 A^{2/3}$. The theoretical values are calculated in the RHB model with the DD-ME1 (triangles) [49]and FKVW (dots) density-dependent effective interactions, and with the Gogny interaction in the pairing channel.

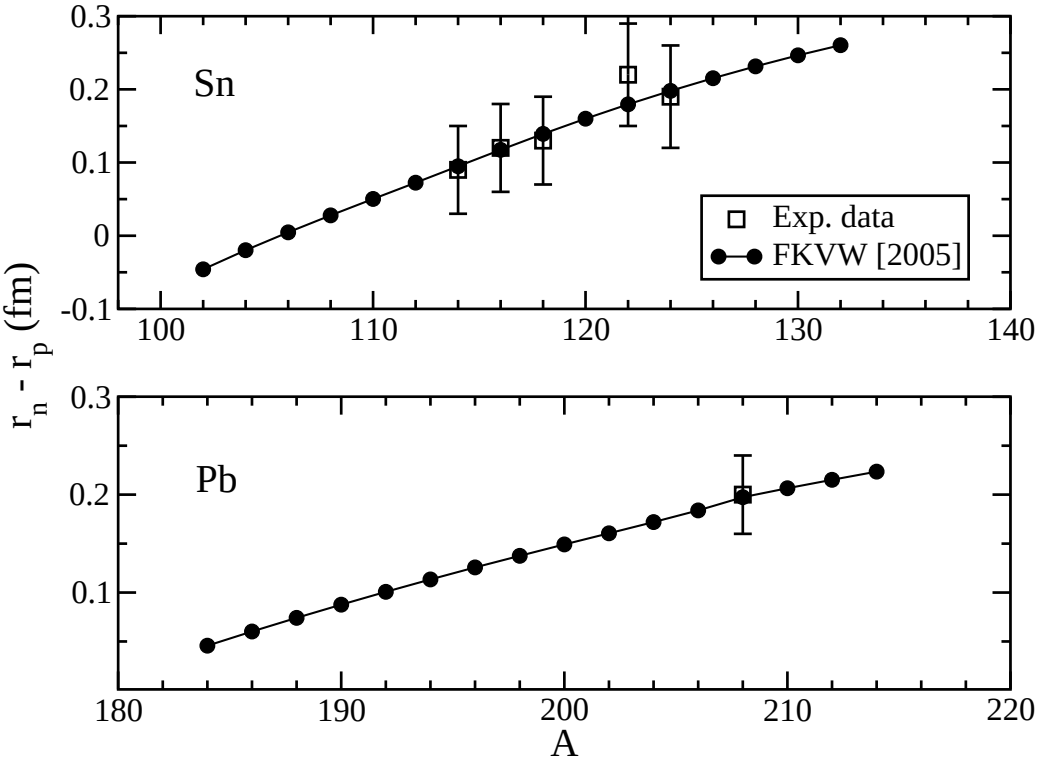

Fig. 6. FKVW plus Gogny RHB-model predictions for the differences between the neutron and proton rms radii of *Sn* (upper panel) and *Pb* (lower panel) isotopes, in comparison with available data [62,63,64].

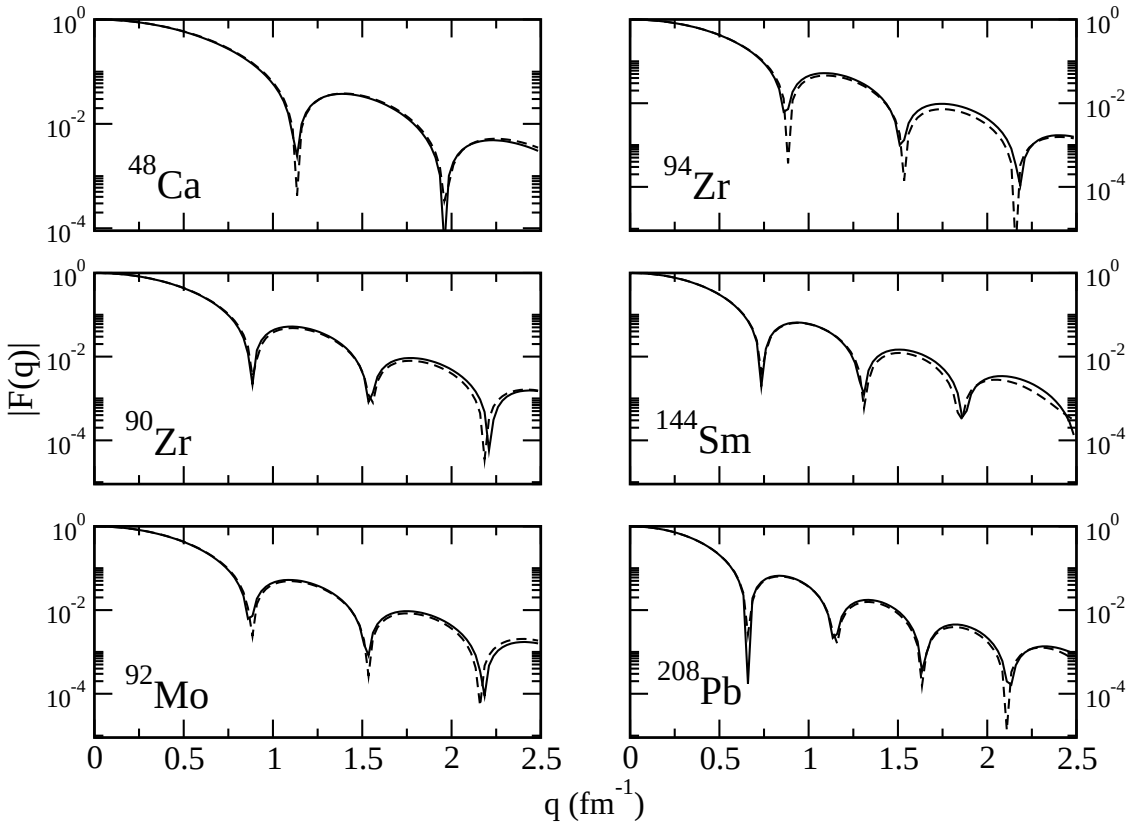

Fig. 7. Charge form factors of ^{48}Ca, ^{90}Zr, ^{92}Mo, ^{94}Zr, ^{144}Sm and ^{208}Pb calculated in the relativistic point-coupling model with the FKVW density-dependent effective interaction (full lines), in comparison with the experimental form factors (dashed lines) [66].

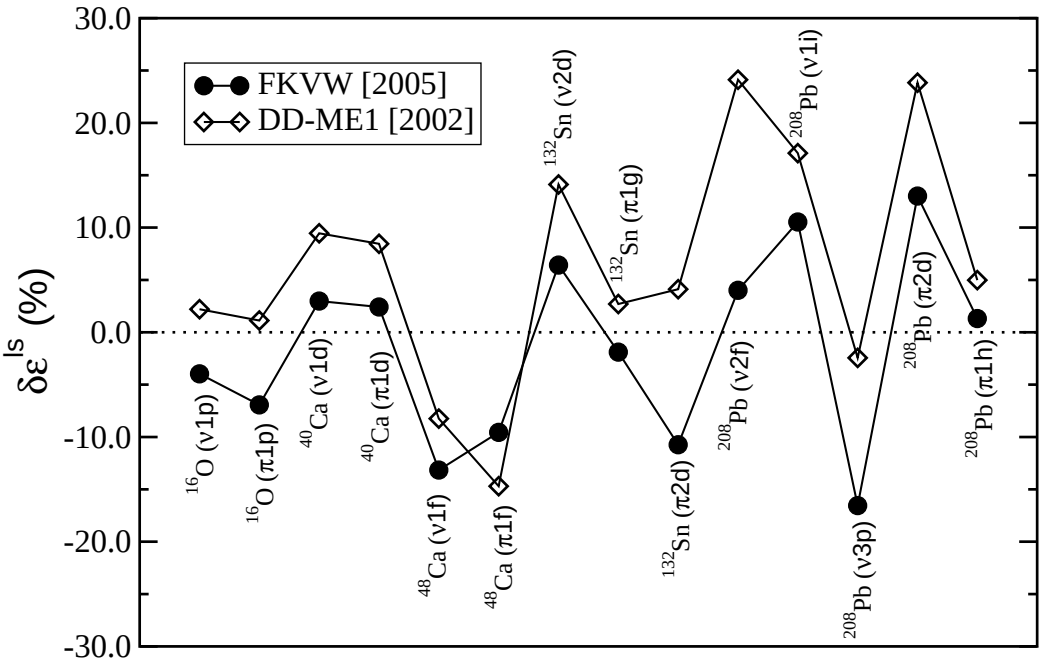

Fig. 8. The deviations (in percent) between the theoretical and experimental values [67] of the energy spacings between spin-orbit partner-states in doubly closed-shell nuclei. The calculated spin-orbit splittings correspond to the relativistic density-dependent point-coupling interaction FKVW (dots), and the relativistic density-dependent meson-exchange interaction DD-ME1 (diamonds) [49].

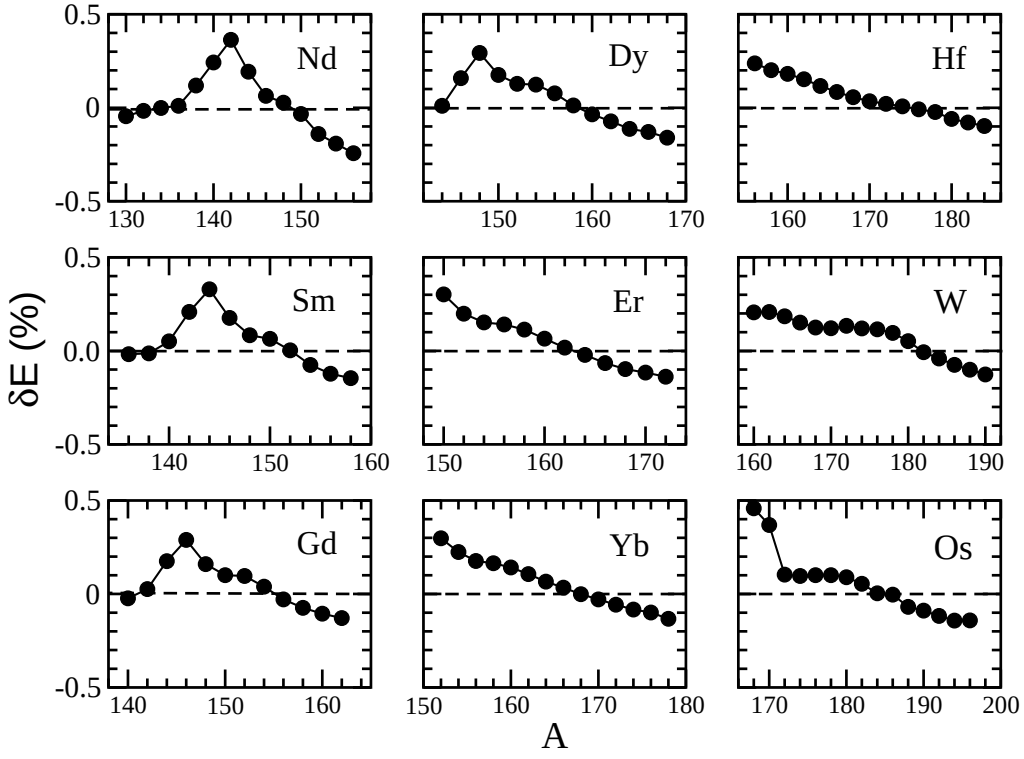

Fig. 9. The deviations (in percent) of the calculated binding energies from the experimental values [57] of Nd, Sm, Gd, Dy, Er, Yb, Hf, W, and Os isotopes. The ground-state binding energies have been calculated in the RHB model with the FKVW parameterization, and with the Gogny interaction in the pairing channel.

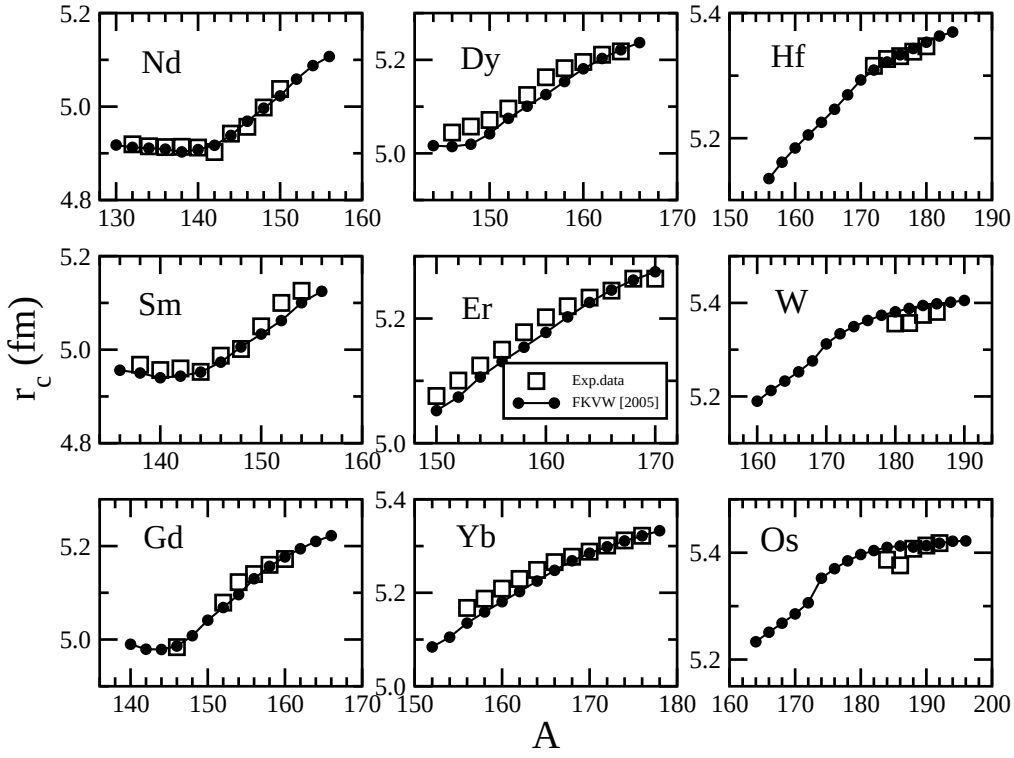

Fig. 10. RHB model (FKVW interaction plus Gogny pairing) predictions for the ground-state charge radii of Nd, Sm, Gd, Dy, Er, Yb, Hf, W, and Os isotopes, in comparison with available data [58].

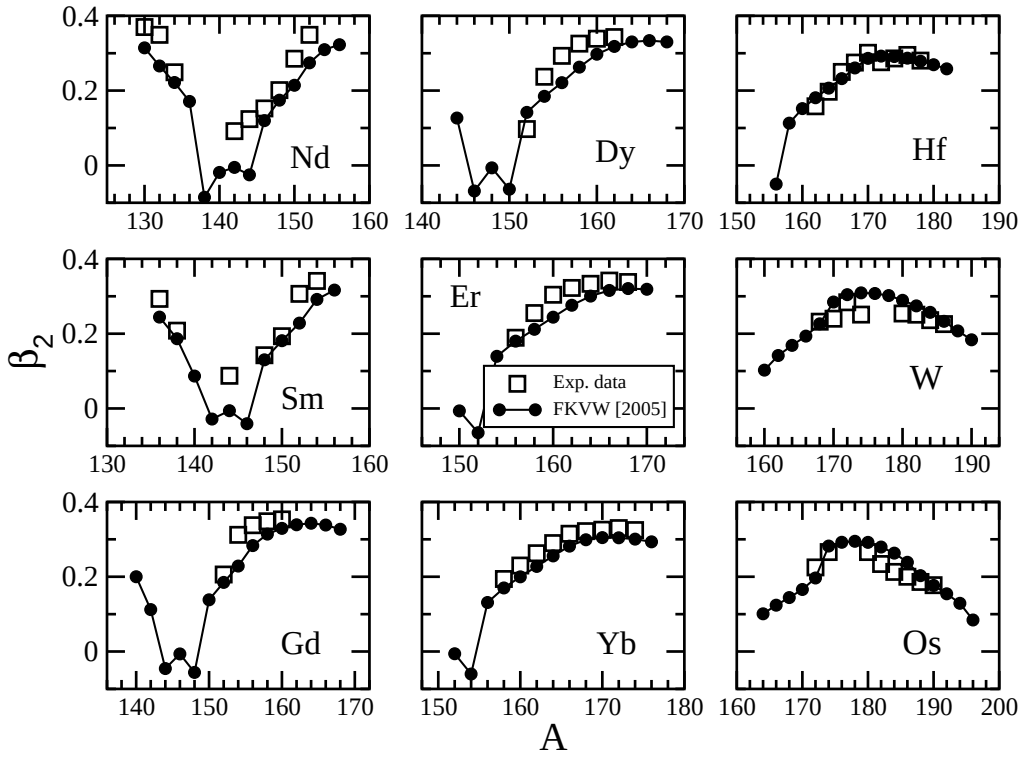

Fig. 11. Comparison between the RHB model (FKVW interaction plus Gogny pairing) predictions for the ground-state quadrupole deformation parameters of the Nd, Sm, Gd, Dy, Er, Yb, Hf, W, and Os isotopes, and experimental values [69].

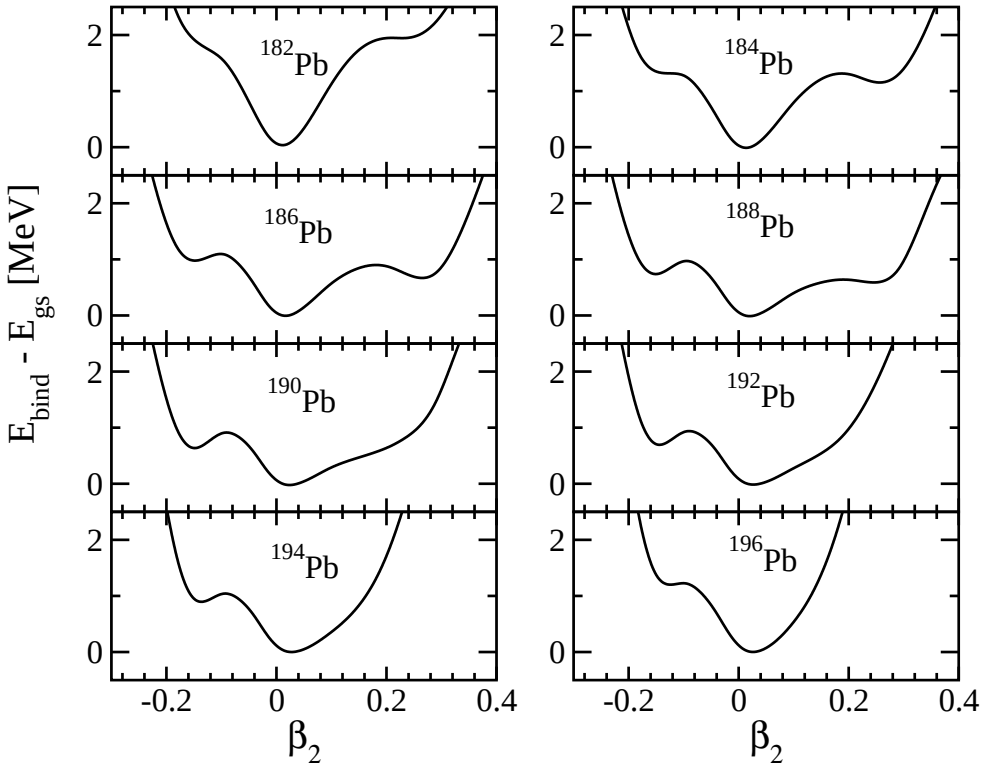

Fig. 12. Binding energy curves of even-A *Pb* isotopes as functions of the quadrupole deformation β_2. The curves correspond to RHB calculations with constrained quadrupole deformation.